

DOT/FAA/AR-07/27

Air Traffic Organization
Operations Planning
Office of Aviation Research
and Development
Washington, DC 20591

Cargo Compartment Smoke Transport Computational Fluid Dynamics Code Validation

July 2007

Final Report

This document is available to the U.S. public
through the National Technical Information
Service (NTIS), Springfield, Virginia 22161.



U.S. Department of Transportation
Federal Aviation Administration

NOTICE

This document is disseminated under the sponsorship of the U.S. Department of Transportation in the interest of information exchange. The United States Government assumes no liability for the contents or use thereof. The United States Government does not endorse products or manufacturers. Trade or manufacturer's names appear herein solely because they are considered essential to the objective of this report. This document does not constitute FAA certification policy. Consult your local FAA aircraft certification office as to its use.

This report is available at the Federal Aviation Administration William J. Hughes Technical Center's Full-Text Technical Reports page: actlibrary.tc.faa.gov in Adobe Acrobat portable document format (PDF).

Technical Report Documentation Page

1. Report No. DOT/FAA/AR-07/27	2. Government Accession No.	3. Recipient's Catalog No.	
4. Title and Subtitle CARGO COMPARTMENT SMOKE TRANSPORT COMPUTATIONAL FLUID DYNAMICS CODE VALIDATION		5. Report Date July 2007	
		6. Performing Organization Code	
7. Author(s) Jill Suo-Anttila, Walt Gill , Anay Luketa-Hanlin, and Carlos Gallegos		8. Performing Organization Report No.	
9. Performing Organization Name and Address Fire Science and Technology Sandia National Laboratories P. O. Box 5800 Albuquerque, NM 87185		10. Work Unit No. (TRAIS)	
		11. Contract or Grant No. DTFA03-00-X-90019	
12. Sponsoring Agency Name and Address U.S. Department of Transportation Federal Aviation Administration Air Traffic Organization Operations Planning Office of Aviation Research and Development Washington, DC 20591		13. Type of Report and Period Covered Final Report	
		14. Sponsoring Agency Code ANM-110	
15. Supplementary Notes The Federal Aviation Administration Airport and Aircraft Safety R&D Division COTR was David Blake.			
16. Abstract A computational model designed to predict smoke and gas transport within aircraft cargo compartments has been validated for potential use in the certification process of cargo compartment fire detection systems. The simulations and experiments compared herein represent a spectrum of scenarios that provide confidence in the models' ability to predict the transport of smoke and combustion products in a variety of conditions. The main variables that changed between the cases were fire location, compartment size, and ventilation. Validation metrics suitable for fire detection system response were selected and, overall, the model favorably predicted these metrics for the selected cases. The model can now be used with improved confidence to simulate certification scenarios of interest to assist in designing the optimum detection systems for cargo compartments.			
17. Key Words Cargo compartment fire detection, Smoke transport model		18. Distribution Statement This document is available to the U.S. public through the National Technical Information Service (NTIS), Springfield, Virginia 22161	
19. Security Classif. (of this report) Unclassified	20. Security Classif. (of this page) Unclassified	21. No. of Pages 64	22. Price

ACKNOWLEDGEMENTS

Sandia National Laboratories is a multiprogram laboratory operated by Sandia Corporation, a Lockheed-Martin Company, for the United States Department of Energy under contract DE-AC04-94AL85000. This project was conducted in collaboration with the Federal Aviation Administration (FAA) William J. Hughes Technical Center, Atlantic City International Airport, NJ, and National Aeronautics and Space Administration (NASA) Glenn Research Center. The work presented in this report was performed by a team of individuals at Sandia National Laboratories and the FAA William J. Hughes Technical Center. Contributions by the following individuals are acknowledged.

Sandia National Laboratories

- Stefan Domino, Anay Luketa-Hanlin, Carlos Gallegos, and Jim Nelsen—Code Development
- Walt Gill—Experimental
- Jill Suo-Anttila—Program Management, Experimental, CFD Analysis
- Lou Gritzo—Program Management, Technical Consultant
- Alex Brown and Carlos Lopez—Document Review

FAA William J. Hughes Technical Center

- David Blake—Program Management, Full-Scale Validation Experiments
- Robert Filipczak and Louise Speitel—Cone Calorimeter Experiments

TABLE OF CONTENTS

	Page
EXECUTIVE SUMMARY	xiii
1. INTRODUCTION	1
2. BACKGROUND	1
3. VALIDATION: METRICS AND COMPARISONS	3
3.1 Selected Metrics for the B-707 Cases	3
3.2 Selected Metrics for the DC-10 Cases	3
4. OVERVIEW OF EXPERIMENTS AND INSTRUMENTATION	4
4.1 B-707 Experimental Description	4
4.2 DC-10 Experimental Description	5
5. COMPUTATIONAL MODEL DESCRIPTION	7
6. MODIFICATIONS PRIOR TO PHASE 2 VALIDATION	9
6.1 Experimental	9
6.2 Computational	9
7. B-707 BASELINE (PHASE 2)	11
7.1 Temperatures	11
7.1.1 Experimental Temperatures	11
7.1.2 Comparison of Experimental and Computational Temperatures	13
7.2 Light Transmission	14
7.2.1 Experimental Light Transmission	14
7.2.2 Computational Light Transmission	17
7.2.3 Comparison of Experimental and Computational Light Transmission	17
7.3 Gas Concentrations	19
7.3.1 Experimental Gas Concentrations	19
7.3.2 Comparison of Experimental and Computational Gas Concentrations	21
7.4 Conclusions for the Baseline B-707 Case	22

8.	B-707 SIDEWALL	22
8.1	Temperatures	22
8.1.1	Experimental Temperatures	22
8.1.2	Comparison of Experimental and Computational Temperatures	23
8.2	Light Transmission	24
8.2.1	Experimental Light Transmission	24
8.2.2	Comparison of Experimental and Computational Light Transmission	25
8.3	Gas Concentrations	26
8.3.1	Experimental Gas Concentrations	26
8.3.2	Comparison of Experimental and Computational Gas Concentrations	27
8.4	Conclusions for the B-707 Attached Sidewall Case	28
9.	B-707 CORNER	28
9.1	Temperatures	28
9.1.1	Experimental Temperatures	28
9.1.2	Comparison of Experimental and Computational Temperatures	30
9.2	Light Transmission	31
9.2.1	Experimental Light Transmission	31
9.2.2	Comparison of Experimental and Computational Light Transmission	32
9.3	Gas Concentrations	34
9.3.1	Experimental Gas Concentrations	34
9.3.2	Comparison of Experimental and Computational Gas Concentrations	34
9.4	Conclusions for the B-707 Attached Corner Scenario	35
10.	DC-10 BASELINE	35
10.1	Temperatures	35
10.1.1	Experimental Temperatures	35
10.1.2	Comparison of Experimental and Computational Temperatures	37
10.2	Light Transmission	38

10.2.1	Experimental Light Transmission	38
10.2.2	Comparison of Experimental and Computational Light Transmission	39
10.3	Gas Concentrations	40
10.3.1	Experimental Gas Concentrations	40
10.3.2	Comparison of Experimental and Computational Gas Concentrations	42
10.4	Conclusions for the DC-10 Baseline Scenario	43
11.	TRANSPORT CODE VARIABLES	43
11.1	Grid	43
11.2	Fire Location	43
11.3	Heat Transfer Coefficient	44
11.4	Time Step Selection	45
12.	CERTIFICATION INSIGHT	46
13.	CONCLUSIONS	46
14.	REFERENCES	47

APPENDIX A—MANUFACTURED SOLUTION VERIFICATION OF FEDERAL
AVIATION ADMINISTRATION SMOKE TRANSPORT CODE

LIST OF FIGURES

Figure		Page
1	Four Classes of Fires	1
2	B-707 Cargo Compartment Fixture Instrumentation	4
3	DC-10 Cargo Compartment Fixture Instrumentation	6
4	B-707 Baseline Computational Mesh	8
5	Example of Computational Output for a B-707 Baseline Case	9
6	Data File	10
7	Experimental Temperature Distribution at 60 Seconds (Average Rise + 293 K)	12
8	Instrumentation Schematic for Baseline Scenario	12
9	B-707 Baseline Ceiling Experimental Temperatures	13
10	Baseline B-707 Temperature Comparison	14
11	B-707 Baseline Experimental Light Transmission Data	16
12	Baseline B-707 Light Transmission Comparison	18
13	B-707 Baseline Experimental Gas Concentrations (CO and CO ₂)	20
14	Baseline B-707 Gas Concentrations Comparison	21
15	Instrumentation Schematic for Sidewall Scenario	22
16	B-707 Sidewall Experimental Temperatures	23
17	B-707 Sidewall Temperature Comparisons	24
18	B-707 Sidewall Experimental Light Transmission	25
19	B-707 Sidewall Light Transmission Comparisons	26
20	B-707 Attached Sidewall Experimental Gas Concentrations	27
21	B-707 Sidewall Gas Concentration Comparisons	28
22	Instrumentation Schematic for Corner Scenario	29
23	B-707 Corner Experimental Temperatures	30

24	Corner B-707 Comparison of Temperatures	31
25	B-707 Attached Corner Experimental Light Transmission	32
26	B-707 Attached Corner Comparison of Light Transmission	33
27	B-707 Attached Corner Experimental Gas Concentrations	34
28	B-707 Attached Corner Comparison of Gas Concentrations	35
29	Schematic of DC-10 Thermocouples and Fire Location	36
30	DC-10 Baseline Experimental Temperatures at 60, 120, and 180 Seconds	37
31	DC-10 Baseline Comparison of Temperatures	38
32	DC-10 Baseline Experimental Light Transmission	39
33	DC-10 Baseline Comparison of Experimental and Computational Light Transmission	40
34	DC-10 Baseline Experimental Gas Concentrations	41
35	DC-10 Comparison of Experimental and Computational Gas Concentrations	42
36	Comparison of Results With Modified Fire Location	44
37	Comparison of B-707 Simulation With Different Heat Transfer Coefficients (60 and 120 Seconds)	45

LIST OF TABLES

Table		Page
1	Phenomenon Identification Ranking Table	2
2	B-707 Instrumentation Locations	5
3	DC-10 Instrumentation Locations	7
4	Experimental Light Transmission Data	15
5	Experimental Gas Concentrations at 60 Seconds	19
6	Experimental Gas Concentrations at 120 Seconds	19
7	Experimental Gas Concentrations at 180 Seconds	19

LIST OF SYMBOLS, ACRONYMS, AND ABBREVIATIONS

CO	Carbon monoxide
CO ₂	Carbon dioxide
CFD	Computational fluid dynamics
FAA	Federal Aviation Administration
FAQ	Frequently asked questions
fwd	Forward
K	Kelvin
kg/s	Kilograms per second
MW	Molecular weight
PIRT	Phenomenon identification ranking table
ppm	Parts per million
TC	Thermocouple
V&V	Verification and validation

EXECUTIVE SUMMARY

Current regulations require that aircraft cargo compartment fire detectors alarm within 1 minute of the start of a fire and at a time before the fire has substantially decreased the structural integrity of the airplane. Presently, in-flight tests, which can be costly and time consuming, are required to demonstrate compliance with the regulations. A physics-based Computational Fluid Dynamics (CFD) tool, which couples heat, mass, and momentum transfer, has been developed to decrease the time and cost of the certification process by reducing the total number of both in-flight and ground experiments. The tool provides information on smoke transport in cargo compartments with varying fire and sensor locations, compartment geometry, ventilation, loading, compartment temperature, and compartment pressure. The fire source term is specified in the model based on Federal Aviation Administration experiments that measured the heat release rate, mass loss rate, and species generation rates of a standardized fire source. The model is fast running, allowing for simulation of numerous fire scenarios in a short period of time, and it is user-friendly, allowing for use by airframe manufacturers and airlines that are not expected to be experts in CFD. This report describes the comparison of a series of experiments and model simulations that provides confidence in the models' ability to predict the transport of smoke and combustion products in a variety of conditions. The main variables in the experiments and simulations were fire location, compartment size, and ventilation. Validation metrics suitable for fire detection system response were selected and, overall, the model favorably predicted these metrics for the selected cases. The model can now be used with improved and documented confidence to simulate certification scenarios of interest to assist in designing the optimum detection systems for cargo compartments.

1. INTRODUCTION.

A computational fluid dynamics (CFD)-based smoke transport code has been developed to improve the aircraft cargo compartment detection system design and certification process. The Federal Aviation Administration (FAA) Smoke Transport code is intended to be used to computationally screen scenarios to determine worst cases, potential detector locations, and alarm thresholds. Before the code can be used in this capacity, it must be thoroughly verified and validated. A verification and validation (V&V) process discussed herein and previously [1] was implemented to both provide confidence in the code for the application of interest, and to identify its limitations.

2. BACKGROUND.

This code was developed in close collaboration with the FAA William J. Hughes Technical Center. From some preliminary experiments conducted, four scenarios of interest were identified, as shown in figure 1. Each class of scenarios corresponds to a different type of fire and compartment-loading configuration. General differences in these fires and loading configurations result in different dominant physical mechanisms of smoke transport. Although the code is capable of simulating compartments with obstacles, it was determined that certification scenarios were of primary interest. Certification is conducted using an empty compartment, thus the validation cases in this report focus on scenario 1 (baseline) and 2 (corner or sidewall) fires in empty compartments only.

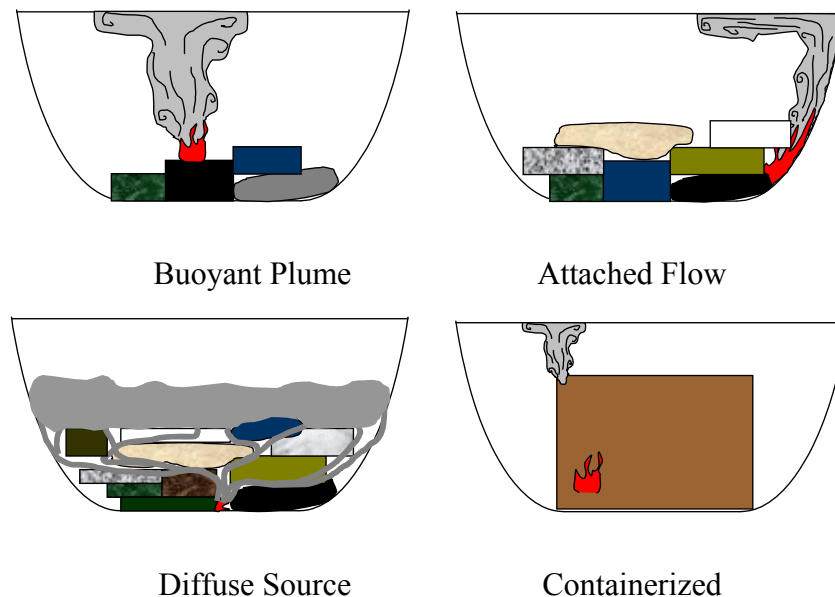


Figure 1. Four Classes of Fires

It was deemed critical that the code contain sufficient fidelity to accurately predict the buoyancy driven transport of fire products. The accuracy of prediction is judged by how well the arrival time of a ceiling jet is captured, and by how well the species concentration as a function of time at any given point is predicted. These are impacted primarily by mixing and species transport in

the buoyant plume. The mechanisms are summarized in the form of a Phenomena Identification and Ranking Table (PIRT) shown in table 1.

Table 1. Phenomenon Identification Ranking Table

Phenomenon	Importance to Outcome
Buoyancy	High
Mixing	High
Species Transport	High
Convection	Med
Combustion	Low

The computational model has been formulated such that dominant mechanisms are accurately simulated, whereas secondary and tertiary effects are either modeled empirically or neglected. Because the code was required to run in a reasonably short time, details of combustion were omitted, and the fire source was specified as heat release, mass release, and species production terms.

The purpose of the model validation is to demonstrate the adequacy of the model for the items in the PIRT and the assumptions in the model are correct. Validation ensures that the right equations are being solved, which is typically done by comparing solutions to experimental data. However, before embarking on a series of experiments and comparisons, it is necessary to ensure the code is solving the equations correctly. This process is known as verification, and it typically relies on comparing results to analytical solutions or derived analytical solutions based on an equivalent source term generation procedure (i.e., manufactured solution). The manufactured solutions approach, a very high-quality verification technique, was used for this model. The verification results were documented in an earlier report [2] and are included in appendix A.

This report describes the validation of the smoke transport model using experimental data acquired in both Boeing-707 and DC-10 cargo compartments. The V&V method implemented here is derived partially from the activities used for verifying and validating Sandia’s fire physics code, FUEGO. Due to constraints and different code requirements, only a subset of the most relevant cases will be used for V&V of the FAA smoke transport code.

Initially, validation experimental data were provided by the FAA William J. Hughes Technical Center for B-707 baseline experiments. These data were analyzed and compared to simulation results as described in reference 1. A number of potential improvements to the experimental data and the simulations were identified; therefore, a second phase of the baseline validation was required. Modifications to both the experiments and the computational code were required prior to completion of the validation.

3. VALIDATION: METRICS AND COMPARISONS.

3.1 SELECTED METRICS FOR THE B-707 CASES.

As stated in the V&V plan, it is desirable to select a scalar quantity that represents a quantity of interest to the ultimate user when comparing experimental and computational results. Based upon a previous analysis and input from project participants, the following have been selected as validation metrics.

- Thermocouple temperature rise from 0-60 seconds, 0-120 seconds, and 0-180 seconds
- Light transmission
 - 30 and 45 seconds (ceiling and vertical)
 - 60 seconds (vertical—high, mid, low)
 - 120 seconds (vertical—mid and low)
 - 180 seconds (vertical—mid and low)
- Gas species concentration rises at 60, 120, and 180 seconds

Note that light transmission comparisons were selected at times and locations such that the experimental measurement was above 80%, since the uncertainty of the diagnostic increases greatly below that threshold.

3.2 SELECTED METRICS FOR THE DC-10 CASES.

After a detailed analysis, the following have been selected as validation metrics for the DC-10 scenarios. As in the B-707 case, light transmission comparisons were selected such that the experimental measurement was above 83%, since the uncertainty of the diagnostic increases greatly below that threshold due to the long path length in the DC-10 compartment.

- Thermocouple temperature rise from 0-60 seconds, 0-120 seconds, and 0-180 seconds
- Light transmission
 - 30 seconds (forward, mid, aft, 5')
 - 45 seconds (forward, mid, aft, 5')
 - 60 seconds (forward, mid, aft, 5')
 - 90 seconds (mid, aft, 5')
 - 120 seconds (mid, aft)
 - 180 seconds (mid, aft)
- Gas species concentration rises at 60, 120, and 180 seconds

4. OVERVIEW OF EXPERIMENTS AND INSTRUMENTATION.

4.1 B-707 EXPERIMENTAL DESCRIPTION.

The experimental test fixture was equipped with diagnostics to measure the temperature (40 thermocouples), smoke obscuration (six smokemeters), heat flux (two sensors), and gas species concentrations. Figure 2 shows the B-707 test fixture instrumentation. A ventilation duct is shown in the photograph, but typical ventilation rates were too low to impact the results; therefore, all B-707 cases were run without ventilation. The baseline computational mesh clearly indicates the locations of the recessed areas in the B-707 cargo compartment. These three areas are the locations of smoke detectors in this particular compartment. The detectors are placed in the recessed area and are then covered with a screen to prevent baggage from damaging the detectors.

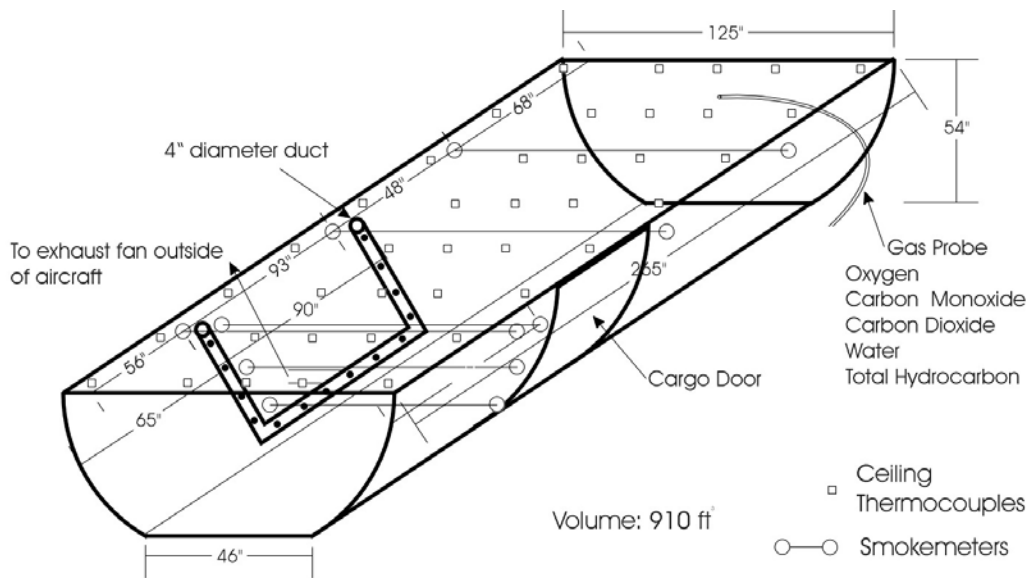


Figure 2. B-707 Cargo Compartment Fixture Instrumentation

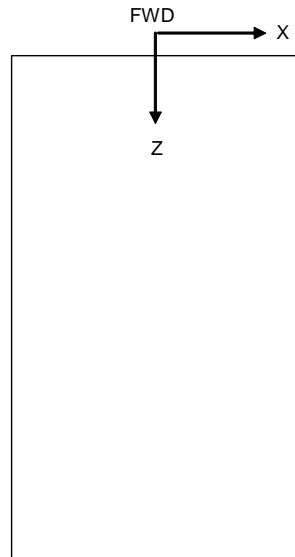
To facilitate comparison with model calculations, the locations of experimental instrumentation in the simulation coordinate system were calculated and tabulated, as shown in table 2. Temperature contours could be created from the sampled points for visualization of the distributions, and actual comparisons of the validation metrics were made point to point.

Table 2. B-707 Instrumentation Locations

707 - Coordinates for Validation Experiments

TC #	X	Y	Z
TC1	-1.37	1.33	0.17
TC2	-0.46	1.33	0.17
TC3	0.00	1.33	0.17
TC4	0.46	1.33	0.17
TC5	1.37	1.33	0.17
TC6	-1.37	1.33	1.08
TC7	-0.46	1.33	1.08
TC8	0.00	1.33	1.08
TC9	0.46	1.33	1.08
TC10	1.37	1.33	1.08
TC11	-1.37	1.33	1.99
TC12	-0.46	1.33	1.99
TC13	0.00	1.33	1.99
TC14	0.46	1.33	1.99
TC15	1.10	1.33	1.99
TC16	-1.37	1.33	2.91
TC17	-0.46	1.33	2.91
TC18	0.00	1.33	2.91
TC19	0.46	1.33	2.91
TC20	1.10	1.33	2.91
TC21	-1.37	1.33	3.82
TC22	-0.46	1.33	3.82
TC23	0.00	1.33	3.82
TC24	0.46	1.33	3.82
TC25	1.10	1.33	3.82
TC26	-1.37	1.33	4.74
TC27	-0.46	1.33	4.74
TC28	0.00	1.33	4.74
TC29	0.46	1.33	4.74
TC30	1.37	1.33	4.74
TC31	-1.37	1.33	5.65
TC32	-0.46	1.33	5.65
TC33	0.00	1.33	5.65
TC34	0.46	1.33	5.65
TC35	1.37	1.33	5.65
TC36	-1.37	1.33	6.57
TC37	-0.46	1.33	6.57
TC38	0.00	1.33	6.57
TC39	0.46	1.33	6.57
TC40	1.37	1.33	6.57
ceil smk fwd	(-1.58 to 1.58)	1.3	1.73
ceil smk mid	(-1.58 to 1.58)	1.3	2.95
ceil smk aft	(-1.58 to 1.58)	1.3	5.31
vert smk high	(-1.51 to 1.51)	1.02	4.90
vert smk mid	(-1.39 to 1.39)	0.74	4.90
vert smk low	(-1.04 to 1.04)	0.33	4.90
Gas mid	0.00	1.42	3.23
Gas aft	0.00	1.42	4.75
Gas TC36	-1.32	1.35	6.52

Coordinates in meters



Compartment Dimensions

L(z)	6.73	
H(y)	1.45	includes 3" recessed area
W(x1)	1.17	
W(x2)	3.18	

Fire Locations	Baseline	Attached	Corner
x	0.08	0.43	0.43
z	3.73	1.8	0.28

Recessed Areas (approximate center)

x1	0
z1	2.3
x2	0
z2	3.3
x3	0
z3	4.7

TC = thermocouple
 ceil = Ceiling
 smk = smokemeter
 vert = vertical

fwd = Forward
 L = Length
 H = Height
 W = Width

4.2 DC-10 EXPERIMENTAL DESCRIPTION.

The wide-body cargo compartment (DC-10) experimental test fixture was equipped with diagnostics to measure the temperature (45 thermocouples), smoke obscuration (four smokemeters), and gas species concentrations. Figure 3 shows the DC-10 cargo compartment test fixture instrumentation. The cargo compartment contains forced air ventilation that enters at

a significantly higher rate than in an operational B-707 (since the B-707 has no forced ventilation). In general, the ventilation enters through two ports in the ceiling and exits through the door seal. Performing experiments in this large, ventilated compartment allows the model to be validated for different scenarios. Note that the compartment only contains two recessed areas and most instrumentation is concentrated in half the compartment.

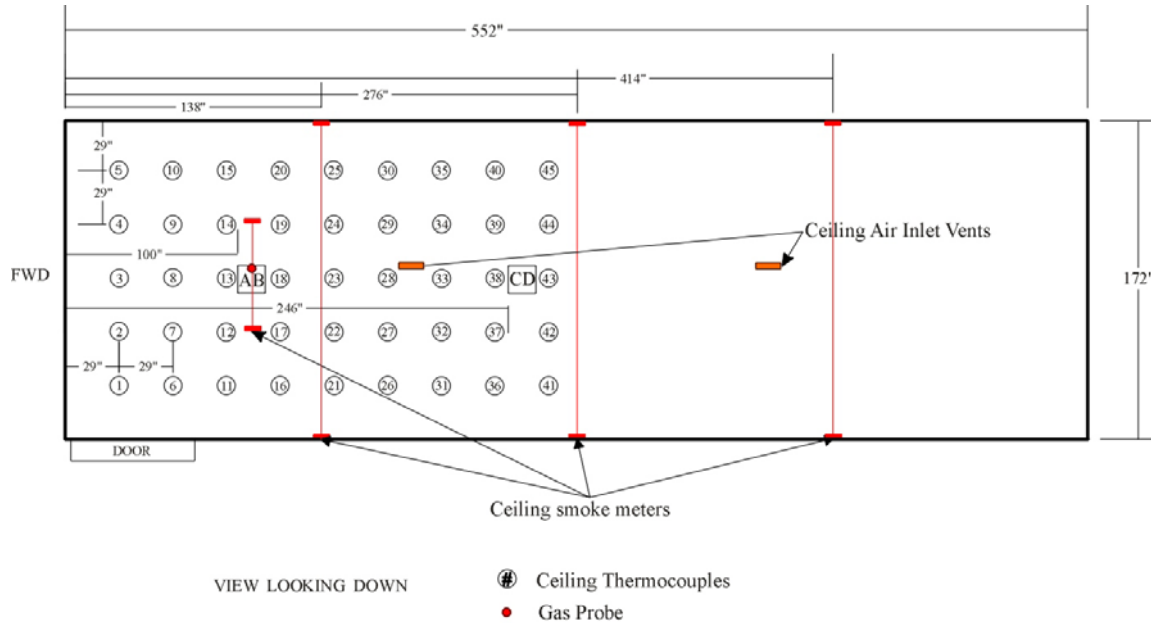


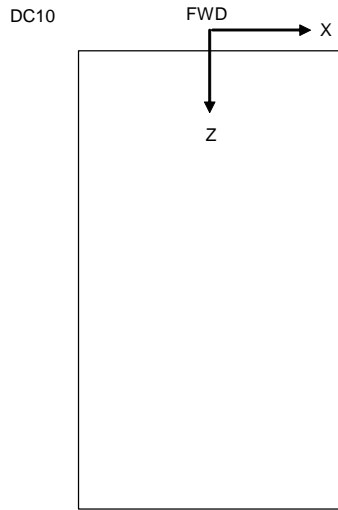
Figure 3. DC-10 Cargo Compartment Fixture Instrumentation

To facilitate comparison with model calculations, the locations of experimental instrumentation in the simulation coordinate system were calculated and tabulated, as shown in table 3. Similar to the B-707 results, temperature contours could be created from the sampled points for visualization of the distributions, whereas actual comparisons of the validation metrics were made point to point.

Table 3. DC-10 Instrumentation Locations

DC-10 mid cargo compartment			
TC #	X	Y	Z
TC1	-1.4986	1.65	0.74
TC2	-0.7620	1.65	0.74
TC3	-0.0254	1.65	0.74
TC4	0.7112	1.65	0.74
TC5	1.4478	1.65	0.74
TC6	-1.4986	1.65	1.47
TC7	-0.7620	1.65	1.47
TC8	-0.0254	1.65	1.47
TC9	0.7112	1.65	1.47
TC10	1.4478	1.65	1.47
TC11	-1.4986	1.65	2.21
TC12	-0.7620	1.65	2.21
TC13	-0.0254	1.65	2.21
TC14	0.7112	1.65	2.21
TC15	1.4478	1.65	2.21
TC16	-1.4986	1.65	2.95
TC17	-0.7620	1.65	2.95
TC18	-0.0254	1.65	2.95
TC19	0.7112	1.65	2.95
TC20	1.4478	1.65	2.95
TC21	-1.4986	1.65	3.68
TC22	-0.7620	1.65	3.68
TC23	-0.0254	1.65	3.68
TC24	0.7112	1.65	3.68
TC25	1.4478	1.65	3.68
TC26	-1.4986	1.65	4.42
TC27	-0.7620	1.65	4.42
TC28	-0.0254	1.65	4.42
TC29	0.7112	1.65	4.42
TC30	1.4478	1.65	4.42
TC31	-1.4986	1.65	5.16
TC32	-0.7620	1.65	5.16
TC33	-0.0254	1.65	5.16
TC34	0.7112	1.65	5.16
TC35	1.4478	1.65	5.16
TC36	-1.4986	1.65	5.89
TC37	-0.7620	1.65	5.89
TC38	-0.0254	1.65	5.89
TC39	0.7112	1.65	5.89
TC40	1.4478	1.65	5.89
TC41	-1.4986	1.65	6.63
TC42	-0.7620	1.65	6.63
TC43	-0.0254	1.65	6.63
TC44	0.7112	1.65	6.63
TC45	1.4478	1.65	6.63
ceil smk fwd	2.1844, -2.1844	1.63	3.51
ceil smk mid	2.1844, -2.1845	1.63	7.01
ceil smk aft	2.1844, -2.1846	1.63	10.52
5' ceil smoke	0.7366, -0.7366	1.65	2.72
Gas fwd	0.0508	1.70	2.67
Gas aft	0.0508	1.70	6.43
Gas T/C 5	1.4478	1.65	0.74

Coordinates in meters



Compartment Dimensions

L(z)	14.02
H(y)	1.73 includes 2" recessed area
W(x1)	3.38
W(x2)	4.39

Fire Locations

	Baseline
x	-0.0762
z	3.302

Recessed Areas (approximate center)

x1	0	
z1	2.72	
x2	0	
z2	6.43	

Ventilation

Outlet	door - see drawing	9" = 0.23 m
Inlets	#1	0 4.69
	#2	0 9.51
		(to center of inlet)

TC = thermocouple
 ceil = Ceiling
 smk = smokemeter

fwd = Forward
 L = Length
 H = Height
 W = Width

5. COMPUTATIONAL MODEL DESCRIPTION.

Computational simulations were performed for comparison to the experiments to facilitate validation of the computational model. A typical computational mesh for the B-707 cargo compartment, consisting of approximately 24 by 20 by 37 nodes, is shown in figure 4. The geometry of the cargo compartment is accurately represented by the body-fitted coordinate system of the computational model. The mesh includes refined regions and three recessed areas. The computational model runs on a standard personal computer, Linux[®] workstation, and

Solaris[®] workstation. Simulations were run using a 1.8 GHz Dell[®] Latitude[®] laptop (Microsoft[®] Windows[®] operating system), taking approximately 1 hour of computational run time for each minute of real time (using a time step of 0.1 second.)

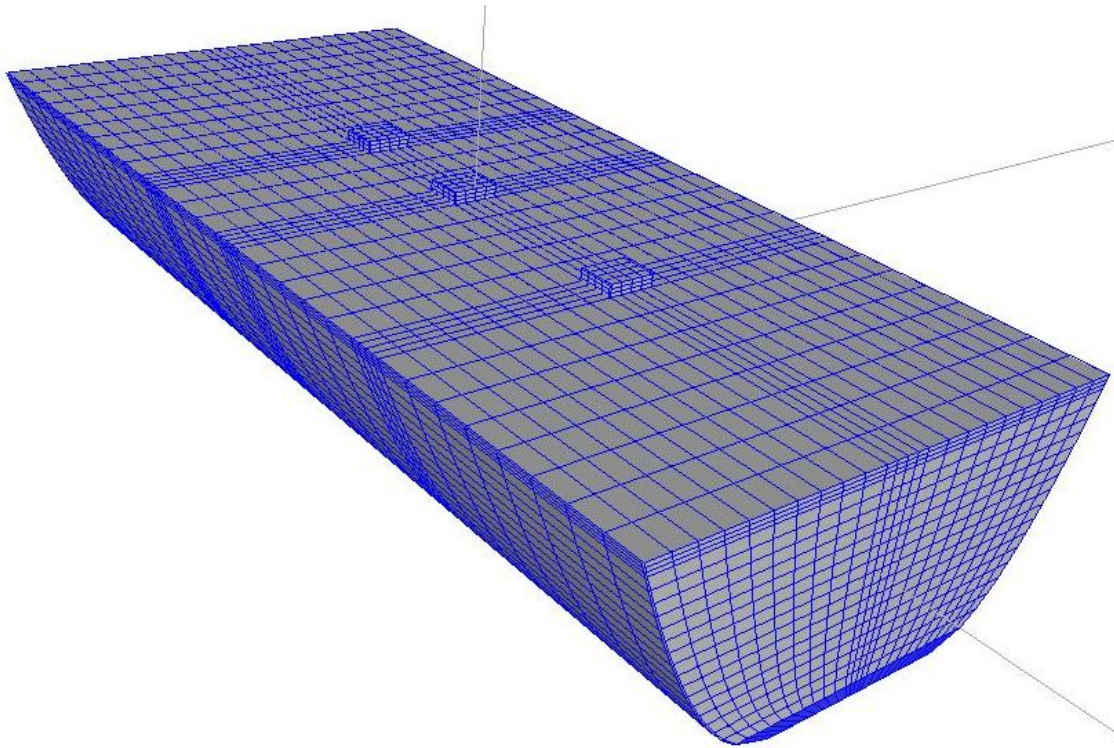


Figure 4. B-707 Baseline Computational Mesh

A flaming fire event occurring over 300 seconds was simulated using the computational model. The specification of the flaming fire source resulted from extensive cone calorimeter experiments at the FAA William J. Hughes Technical Center [3]. The fire is specified as a source term as measured during these detailed FAA experiments. The average of the three flaming fire data sets was used as the source term for the calculations.

Extensive data within the computational domain result from the simulation. For each time step, at each of the cells in the computational domain, the user has access to values of flow velocity (u , v , w), density, temperature, turbulence parameters, and species concentrations. An example of the temperature results (for a B-707 baseline simulation) within a plane of the computational domain is shown in figure 5. The plane shown is at the centerplane of the fire, and the progression of the ceiling jet and the depth of the smoke layer are visible in the image.

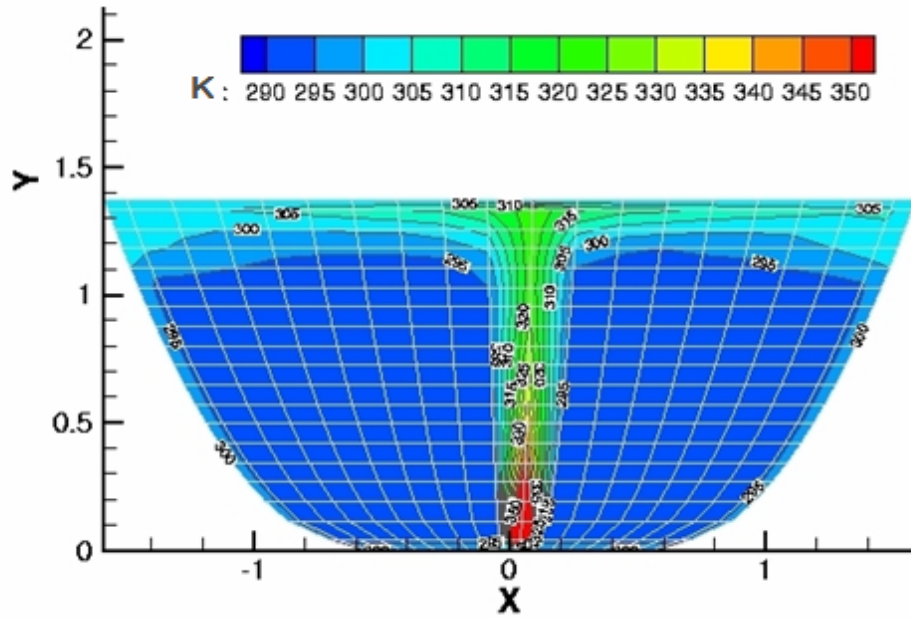


Figure 5. Example of Computational Output for a B-707 Baseline Case (Temperature in K)

6. MODIFICATIONS PRIOR TO PHASE 2 VALIDATION.

This report presents the phase 2 validation effort for the FAA Smoke Transport code. The initial validation, referred to as phase 1, was documented previously [1]. The agreement between the computational and experimental results was unsatisfactory in the phase 1 validation. Issues identified with the model and the experiments were modified prior to the phase 2 validation efforts.

6.1 EXPERIMENTAL.

The two primary modifications to the experimental cargo compartment finalized prior to the phase 2 validation experiments were the replacement of sheathed thermocouples with bare junctions and the rerouting of the gas sampling line. These modifications significantly changed the collected experimental data and provided more confidence in the validation metrics.

6.2 COMPUTATIONAL.

Several modifications to the computational code occurred prior to completing the phase 2 validation documented in this report. The first two changes were identified during the phase 1 validation. These included adding the recessed areas to the computational mesh and developing a submodel to account for heat loss to the walls.

In addition to the two modifications described above, several additional changes were required. These are described below.

1. In data file, under the code_files directory, the molecular weights (MW) were changed to reflect that of soot (MW=12), Carbon dioxide (MW=44), Carbon monoxide (MW=28),

and air (MW=28.84). The line where the change is made is highlighted in red (figure 6), which shows the data file.

```
*****
2,                               !nsay
    ***test plume with thermal release rate - no inlet velocity***
    *** faa geometry Soot, CO2, and CO with adiabatic walls ***
F, T, T, T, T                    !simpler, lturb, lscalar, lenergy, lvary
8.5, 10, 1, 4                    !sormax, n_picard, ipp, number_of_species
12.0, 44.0, 28.0, 28.84         !mw_pure (# 1, 2 ...) - molecular weight
.6007e3, .8517e3, 1.043e3, 1.007e3 !cpm_pure(# 1, 2 ...) - heat capacity
0.0, 0.0                          !spm_i, sph_i: kg/s; joule/s
0.0, 0.0, 0.00, 0.0              !mass f. of species stream (# 1, 2 ...)
1.0                                !adiabtw; = 1, adiabatic walls, = 0 heat loss
0.90, 0.90, 0.90                 !urfv, v , w
1.00, 1.00, 0.85                 !urftpp, p, fl
0.85, 0.85, 1.00                 !urftf2, f3, te
1.00, 0.85, 0.85                 !urfed, h, den/props
                                !blank line
*****
```

Figure 6. Data File

- Source terms for soot, carbon monoxide (CO), and carbon dioxide (CO₂) were changed in the rates.dat file. They were changed to be normalized by the mass release rate of fuel only instead of by the sum of the mass release rate of fuel and air. This was changed for consistency. In the code the source terms were being renormalized by just the mass release rate of fuel in order to arrive at a species source term in units of kilograms per second (kg/s). Thus, before the change, the renormalized source terms in units of kg/s were lower than what they should have been by almost a factor of 2.

Note that the source term values in the rates.dat file should be considered as normalized values rather than mass fractions since the sum of mass fractions are typically regarded to equal 1. The source term values in the rates.dat file now exceed 1 since the values are not normalized by the total mass in the system.

- The line in the code that initializes the volume of air in the cabin was changed in line 274 of the sand_head.f file. The mw_pure value for species (2) (CO₂) was being used instead of mw_pure(4) for air

from:

$$\text{mass_initial} = \text{total_v} * \text{mw_pure}(2) / (0.08206 * (\text{h}(23) / \text{cvfl}))$$

to:

$$\text{mass_initial} = \text{total_v} * \text{mw_pure}(4) / (0.08206 * (\text{h}(23) / \text{cvfl}))$$

- The formulation for interpolation was modified to reflect a linear interpolation in the data_interpolation.f file

from:

$$\begin{aligned}m &= \text{data_m}(\text{count2}) - \text{data_m}(\text{count1}) \\b &= \text{data_m}(\text{count1}) \\x &= \text{time} \\ \text{spm_i} &= m * x + b\end{aligned}$$

to:

$$\begin{aligned}m &= \text{data_m}(\text{count2}) - \text{data_m}(\text{count1}) \\b &= \text{data_m}(\text{count1}) - m * \text{count1} \\x &= \text{time} \\ \text{spm_i} &= m * x + b\end{aligned}$$

5. Note that during postprocessing in the Excel file, result.xls, the species in units of ppm were calculated by:

$$\text{Species (ppm species/ppm air)} = \text{species (kg/kg)} * 1e6 * \text{density of air} / \text{density of species}$$

where,

$$\text{Density of species} = \text{pressure} * \text{MW} / (\text{R} * \text{T})$$

The temperature, T, was evaluated at the nearest thermocouple reading instead of at a constant temperature of 293K.

6. For the DC-10 case, line 37 in subroutine modvel.f was modified by changing iblock = .false. to iblock = .true. Before this change there was no outflow through the cabin door; thus, there was a buildup of pressure and the density was increasing by a factor of 2 above atmospheric.

[7. B-707 BASELINE \(PHASE 2\).](#)

[7.1 TEMPERATURES.](#)

[7.1.1 Experimental Temperatures.](#)

The method chosen for using thermocouple data was to compare the temperature rise at 60, 120, and 180 seconds. Comparison of the absolute temperature at a time after ignition is not practical due to different initial temperatures of the cargo compartment. To perform the temperature comparisons, the experimental data from each thermocouple were analyzed. The average temperature rise and the standard deviation for a thermocouple was calculated using data from all phase 2 baseline experiments (15 total). To obtain a temperature for the comparison, the average temperature rise was added to the initial temperature of the calculation domain. A contour plot of the temperature distribution of an early simulation (not the final baseline simulation) is shown in figure 7. The circles on the plot denote the thermocouple locations where the temperatures were measured. Temperatures at all other locations were determined by the linear interpolation function in the Tecplot[®] graphics package. The maximum temperature of 308 Kelvin (K) is

recorded by the thermocouple closest to the point directly above the fire source. The temperatures decrease with radial distance from the fire source and the thermocouples in the extreme forward and aft area recorded near-ambient temperatures.

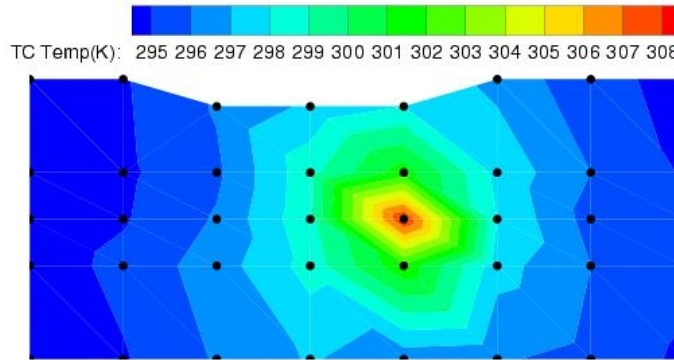


Figure 7. Experimental Temperature Distribution at 60 Seconds (Average Rise + 293 K)

To assist in the interpretation of the temperature measurements presented in this section, a schematic of the location of the thermocouples relative to the fire source is provided in figure 8.

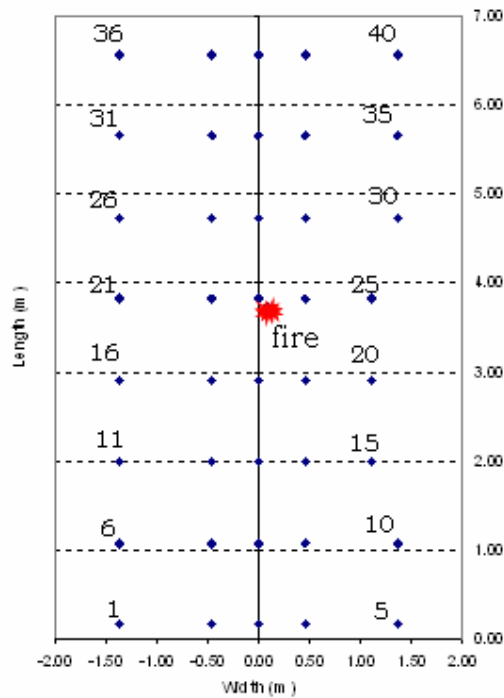


Figure 8. Instrumentation Schematic for Baseline Scenario

Figure 9 displays a scatter plot of the average temperature for each thermocouple at 60, 120, and 180 seconds and the uncertainty associated with the measurement. The error bars represent the 95% confidence interval created using the experimental variation and the instrument drift (0.5 K). As expected, the most variability in the experimental data exists near the fire source

where the uncertainty is ± 6 K at 60 seconds after ignition. The lowest variation in the data of ± 1 K occurs at the locations farthest from the fire source.

Thermocouple temperatures at 120 and 180 seconds display trends in the temperature distribution that are similar to the earlier time. The lowest temperatures are recorded at 60 seconds after ignition. The temperatures are higher at 120 seconds after ignition, but they do not increase much from 120 to 180 seconds after ignition.

Overall, the phase 2 data are higher in temperature due to removal of the sheath surrounding the thermocouple bead. In addition, the trends are different due to rerouting of the gas line, which was altering the transport of hot combustion gases. The phase 2 trends are smoother and much more intuitive.

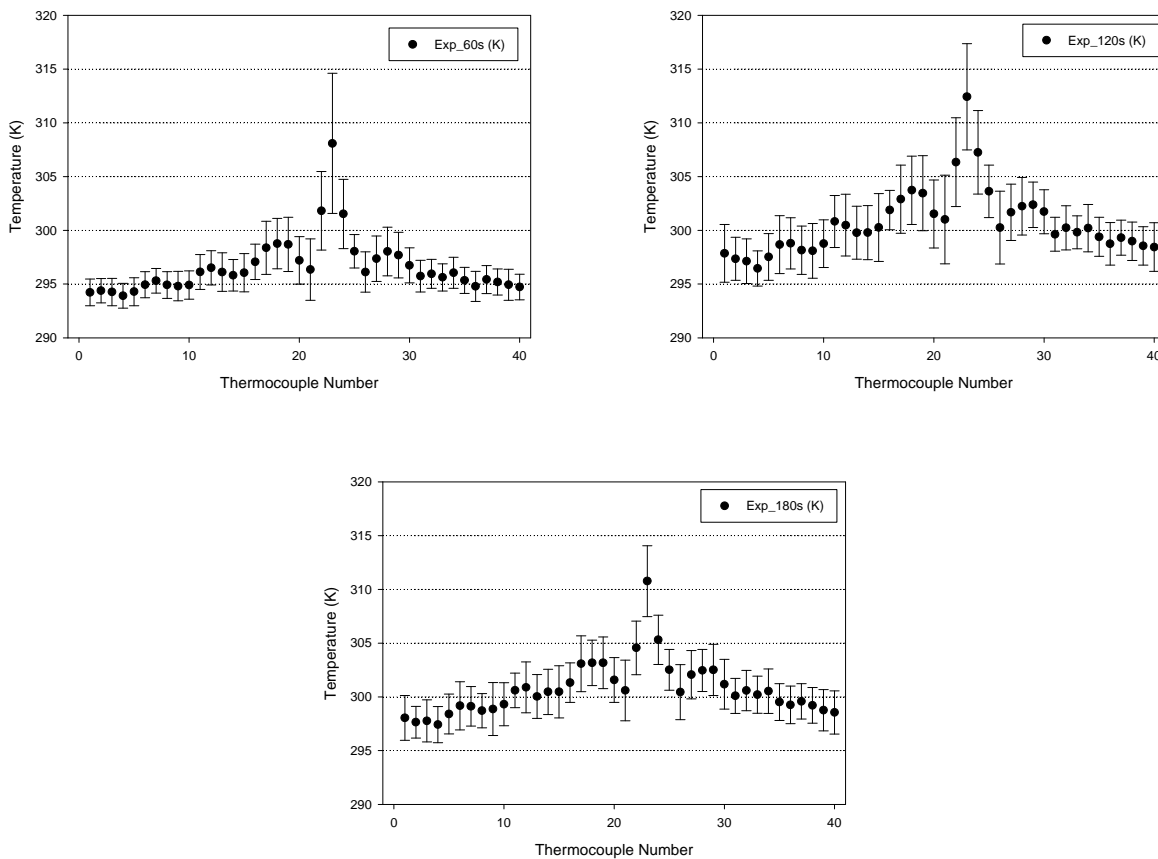


Figure 9. B-707 Baseline Ceiling Experimental Temperatures

7.1.2 Comparison of Experimental and Computational Temperatures.

The computational model predictions are presented in figure 10 for locations corresponding to the experimental thermocouple (TC) locations. At 60 seconds after ignition, the predicted temperatures are similar to the measured temperatures in both the magnitudes and trends. This is encouraging since a detector in a cargo compartment is required to alarm within 60 seconds after fire initiation. By 120 seconds, the trends are still similar, but the magnitudes of the

temperatures, especially near the source, are higher in the predictions. In addition, the highest temperatures are recorded at TC23 and TC24, which have almost the same temperature in the simulations. Due to the refinement of the grid for the recessed areas, the fire location was shifted 0.6" more towards TC24 than in the actual experiments. In the experiments, the highest temperature was recorded by TC23, but there was overlap in the uncertainty bands for TC23 and TC24. This phenomenon also occurred at 180 seconds, although the overall comparisons were favorable.

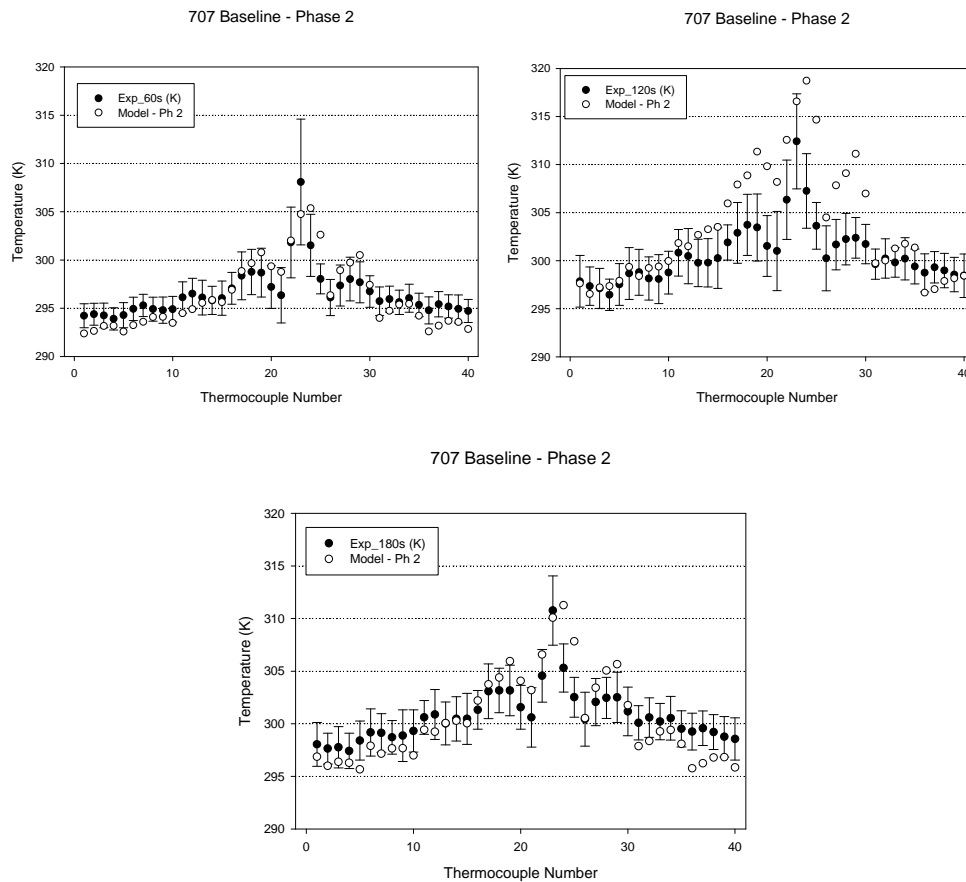


Figure 10. Baseline B-707 Temperature Comparison

7.2 LIGHT TRANSMISSION.

7.2.1 Experimental Light Transmission.

The light transmission was measured experimentally at six locations, as described in table 4. Experimental results are presented in this section. Uncertainty bars have been placed on the experimental measurements, which include the experimental variability, instrument drift, and calibration. The uncertainty due to calibration was 0.4% for all smokemeters. Instrument drifts were 0.1% for ceiling forward, ceiling mid, and vertical mid; 0.4% for vertical high and ceiling aft; and 0.2% for vertical low.

Average smokemeter experimental measurements are shown in table 4. Uncertainty in the operation of the diagnostic is quite high for measurements below 80% light transmission (omitted in table 4); thus, all comparisons were made above this level.

Table 4. Experimental Light Transmission Data

Smokemeter	EXP 30s	EXP 45s	EXP 60s	EXP 120s	EXP 180s
ceil smk fwd	98.7	92.8			
ceil smk mid	95.6	88.7			
ceil smk aft	97.0	90.2			
vert smk high	100.0	99.9	98.3		
vert smk mid	100.0	100.0	100.0	97.3	89.0
vert smk low	100.0	100.0	100.0	100.0	98.7

Figure 11 graphically displays the smokemeter validation metrics. Since the mid smokemeter measurement location is closest to the fire, it responds first. The reading is almost 95% at 30 seconds after ignition. At 30 seconds, the aft smokemeter is attenuated by slightly more smoke than the forward smokemeter, which is consistent with their locations relative to the fire. The three vertical smokemeters have not experienced a decrease in light transmission. This is expected since it is likely the smoke is just spreading across the ceiling in a relatively thin ceiling jet layer. Similar observations can be made at 45 seconds after ignition. The three ceiling smokemeters have similar trends, but their magnitudes have decreased slightly. The three vertical smokemeters are not indicating the presence of smoke.

By 60 seconds after ignition, three upper smokemeters have all dropped below 80% light transmission; therefore, their readings could potentially have a high level of uncertainty associated with them and they are excluded from the plots. The highest smokemeter drops first since the cargo compartment is filling from the top down due to the temperature of the smoke plume. At 120 and 180 seconds, the mid and low vertical smokemeters respond, indicating that the compartment is filling with a considerable amount of smoke from the top down.

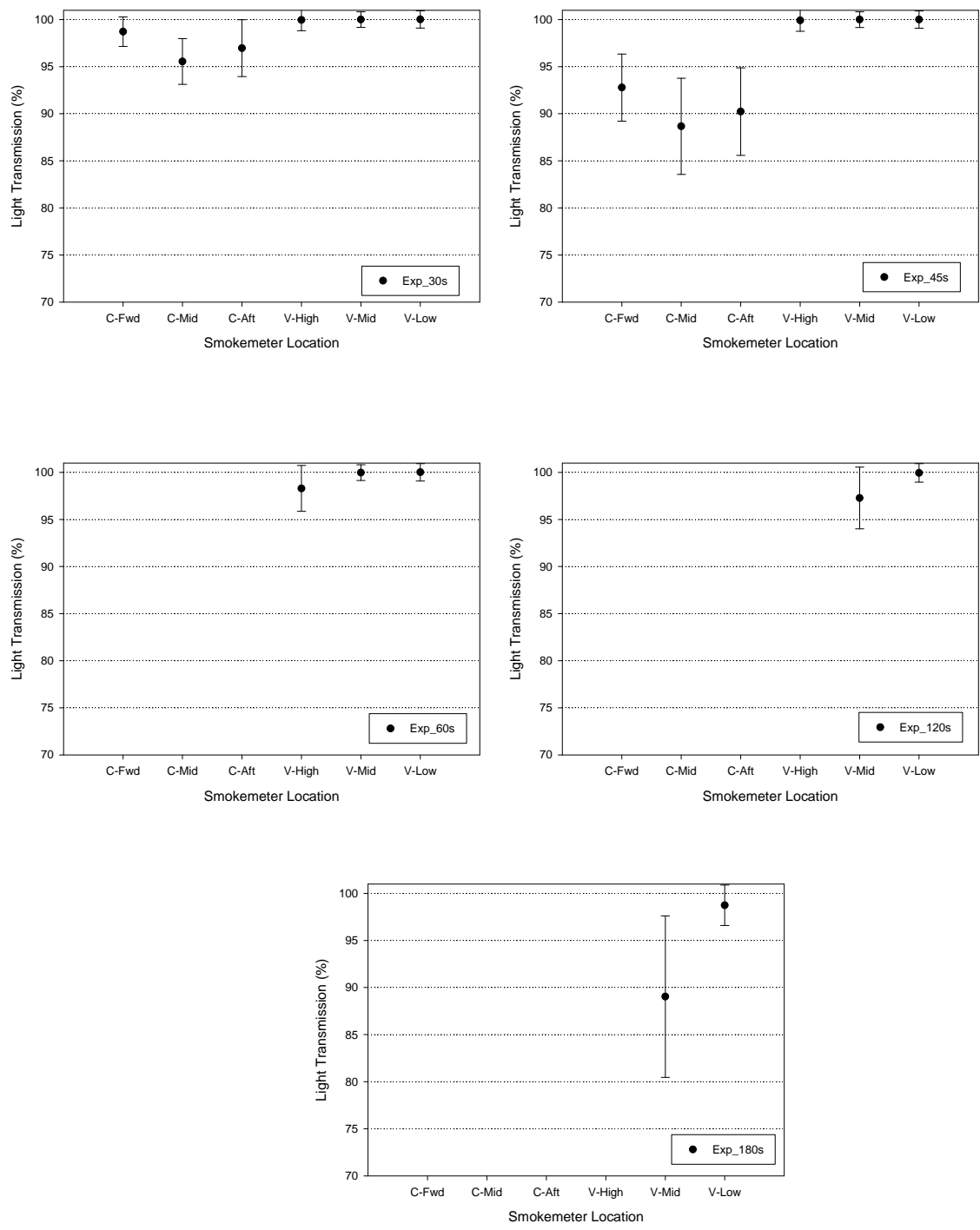


Figure 11. B-707 Baseline Experimental Light Transmission Data

7.2.2 Computational Light Transmission.

Light transmission is not directly calculated in the computational model; instead, the model results are postprocessed to determine the light transmission at the time of interest.

Smokemeter readings were calculated by integrating soot concentration information for the cells located along the beam path. Output from individual computational cells was used to determine percent light transmission (the value measured in the experiments) for the predicted field values using Beer's Law.

$$\frac{I}{I_0} = e^{-\int_0^L k(x) dx} \quad \text{where } k(x) = C_{soot}(x) \rho_{cell}(x) \sigma_s$$

where σ_s is the specific extinction coefficient ($7400 \frac{m^2}{kg}$), C_{soot} is the soot concentration ($\frac{kg}{kg}$), and ρ_{cell} is the gas density ($\frac{kg}{m^3}$).

The specific extinction coefficient value is based upon earlier research on the soot morphology and optical properties. The coefficient was determined using the soot morphology from the flaming resin and the Rayleigh-Debye-Gans theory for polydisperse fractal aggregates.

The values for C_{soot} and ρ_{cell} are output for each cell at each time step in the simulation. A computer code was written to perform the calculation for the decrease in light transmission from the sum of the individual cells along the beam path of the smokemeter. In accordance with the procedure used by the FAA, the intensity ratio was then raised to the $1/L$ power (with L in feet).

$$LT\% / ft = 100 \cdot \left(\frac{I}{I_0} \right)^{\frac{1}{L}} = 100 \cdot e^{-\frac{\int_0^L k \cdot dx}{L}}$$

7.2.3 Comparison of Experimental and Computational Light Transmission.

As discussed in section 7.2.1, the light transmissions at 30, 45, 60, 120, and 180 seconds were compared (see figure 12). Overall, the model did an excellent job of predicting the light transmission at times before 60 seconds (the required alarm time). The model predictions fell outside the experimental uncertainty bands at 120 and 180 seconds, although the trends were still well predicted.

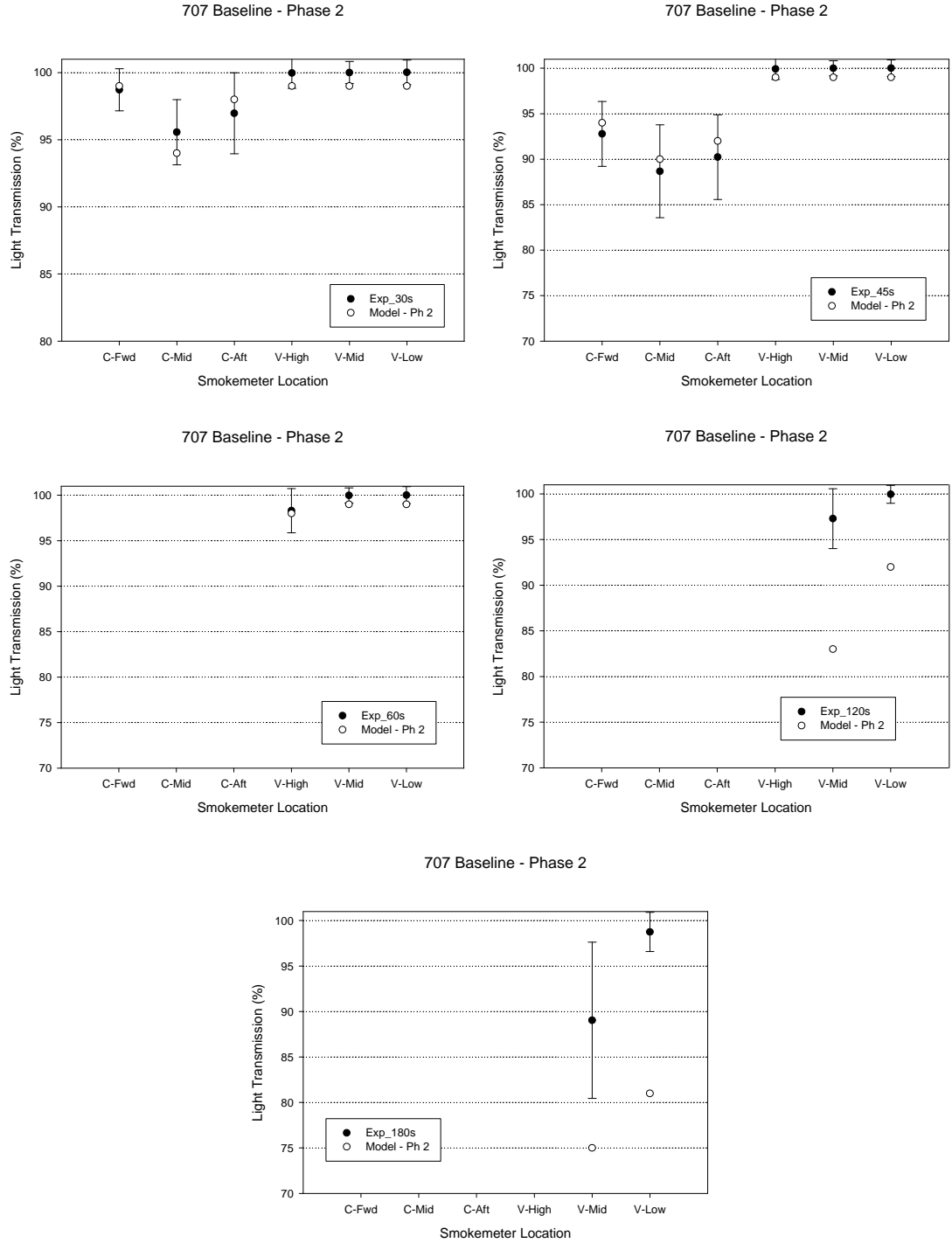


Figure 12. Baseline B-707 Light Transmission Comparison

7.3 GAS CONCENTRATIONS.

7.3.1 Experimental Gas Concentrations.

The average rise in experimental gas concentrations from five replicate experiments was computed at 60, 120, and 180 seconds after ignition. The results are shown in tables 5 through 7, and graphs are shown in figure 13. The total uncertainty (95% confidence interval) in the experimental results includes experimental variability, instrument accuracy, and instrument drift. The accuracy of the instrument was obtained from the manufacturer as $\pm 1\%$ of the range. The range for CO was 500 parts per million (ppm), and the range for CO₂ was 2500 ppm. The drift was determined using results from a series of early experiments.

Table 5. Experimental Gas Concentrations at 60 Seconds (in ppm)

60 sec.	EXP_Ph2	σ	($\pm 1\%$ range)	Drift	Uncert. bar
CO – mid	94.0	11.4	5.0	0.3	25.0
CO ₂ – mid	892.9	88.8	25.0	3.5	184.7
CO – aft	78.2	6.4	5.0	0.3	16.3
CO ₂ – aft	724.8	39.7	25.0	3.5	94.2
CO – TC36	14.7	343.1	5.0	0.3	686.3
CO ₂ – TC36	7.2	34.1	25.0	3.5	84.9

Table 6. Experimental Gas Concentrations at 120 Seconds (in ppm)

120 sec.	EXP_Ph2	σ	($\pm 1\%$ range)	Drift	Uncert. bar
CO – mid	110.3	11.8	5.0	0.3	25.6
CO ₂ – mid	1477.9	191.1	25.0	3.5	385.5
CO – aft	96.3	6.4	5.0	0.3	16.2
CO ₂ – aft	1280.3	123.4	25.0	3.5	251.9
CO – TC36	69.9	5.3	5.0	0.3	14.7
CO ₂ – TC36	891.3	53.4	25.0	3.5	118.1

Table 7. Experimental Gas Concentrations at 180 Seconds (in ppm)

180 sec.	EXP_Ph2	σ	($\pm 1\%$ range)	Drift	Uncert. bar
CO – mid	113.4	15.1	5.0	0.3	31.9
CO ₂ – mid	1358.6	212.8	25.0	3.5	428.6
CO – aft	107.1	8.9	5.0	0.3	20.4
CO ₂ – aft	1345.6	164.1	25.0	3.5	332.0
CO – TC36	82.7	3.0	5.0	0.3	11.7
CO ₂ – TC36	1014.5	33.9	25.0	3.5	84.5

Average recorded gas concentrations were consistently highest in the mid pan, followed by the aft pan, and then TC36. Note that there is overlap within the measurement uncertainty in many cases. The trends in the average values are consistent with the locations of the measurements relative to the fire. Uncertainty in the measurements is significant. A noticeable difference in

the measurement values from the phase 1 experiments was observed, indicating the previous routing of the gas line was impacting the transport of smoke in the cargo compartment.

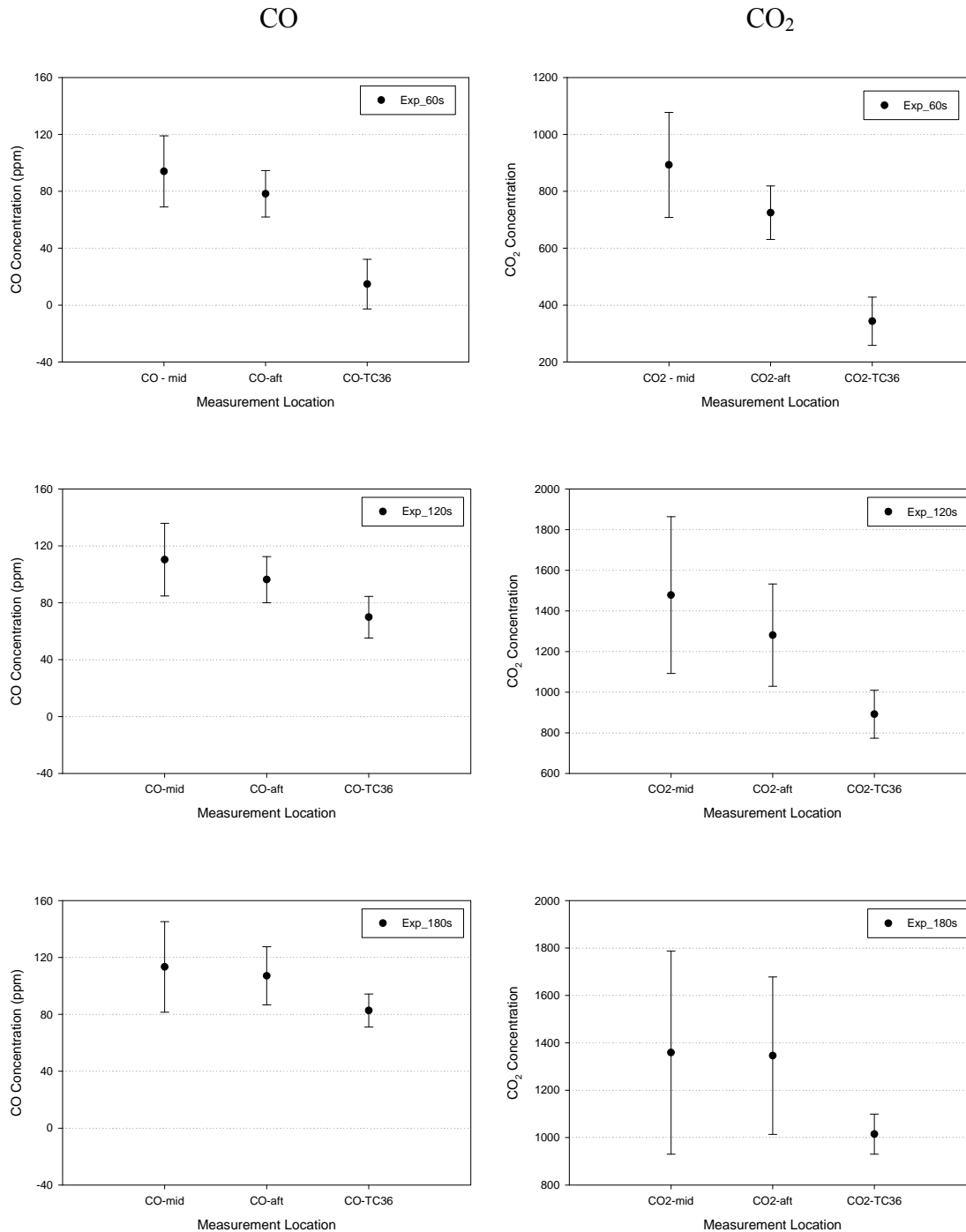


Figure 13. B-707 Baseline Experimental Gas Concentrations (CO and CO₂)

7.3.2 Comparison of Experimental and Computational Gas Concentrations.

Comparison of the gas concentration predictions and the experimental measurements is shown in figure 14. There is very good agreement between the model predictions and the measurements. The predictions fall within the uncertainty bounds for most of the metrics. Overall, the model accurately predicts both the trends and magnitudes of the baseline B-707 gas concentrations.

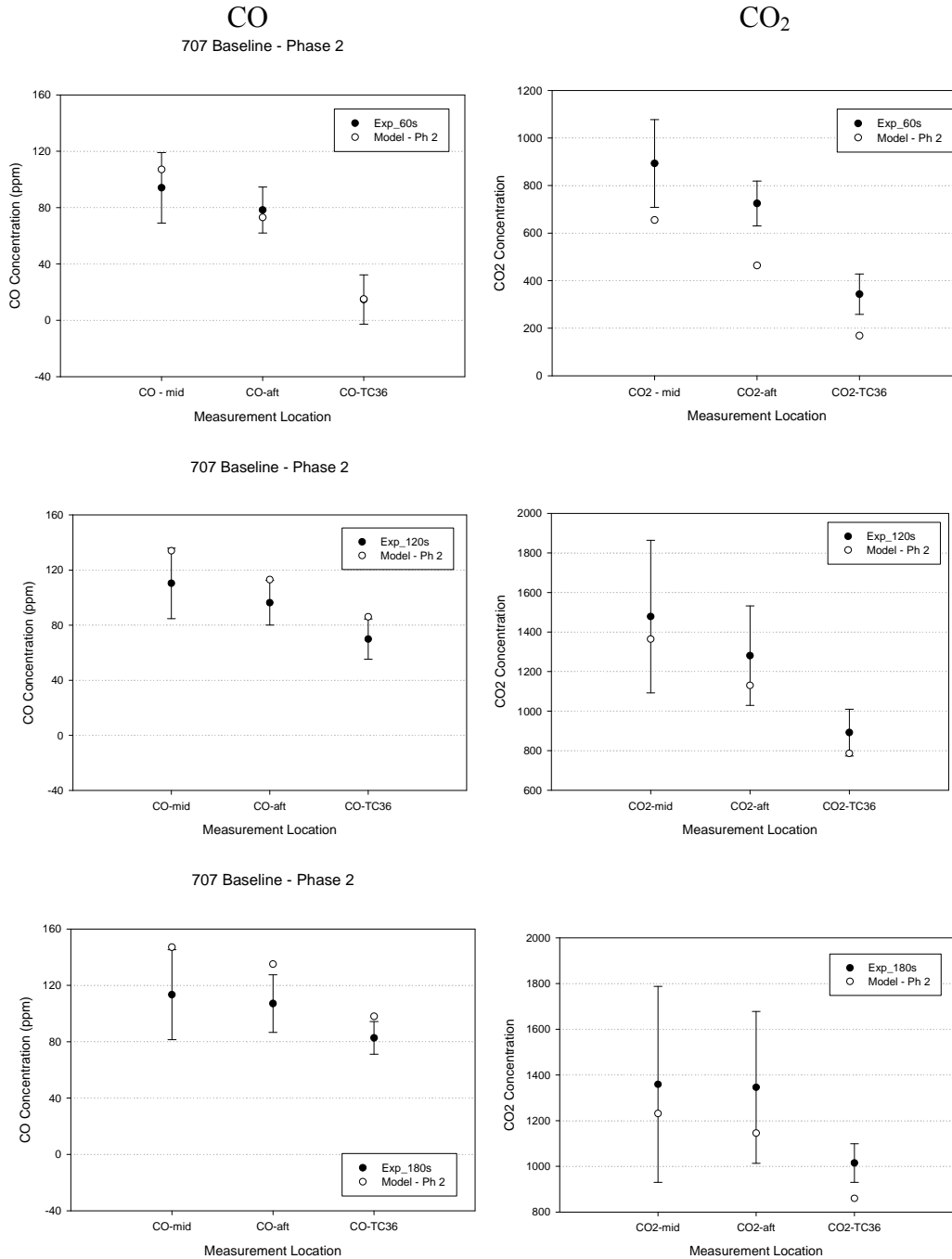


Figure 14. Baseline B-707 Gas Concentrations Comparison

7.4 CONCLUSIONS FOR THE BASELINE B-707 CASE.

Computational model predictions and experimental measurements for the baseline B-707 case were compared in section 7.3. Overall, favorable agreement was observed, especially within the required detection time of 60 seconds. Gas concentration trends and magnitudes were well predicted at all times. Temperature and light transmission magnitudes were better predicted at early times, but the trends were reliably predicted at all times. In conclusion, it should be stated that confidence was gained in the models' ability to predict the transport of heat, smoke, and combustion gases from a fire away from the walls within a lower, unventilated cargo compartment area.

8. B-707 SIDEWALL.

8.1 TEMPERATURES.

8.1.1 Experimental Temperatures.

To assist in the interpretation of the temperature measurements presented in this section, a schematic of the location of the thermocouples relative to the fire source is provided in figure 15.

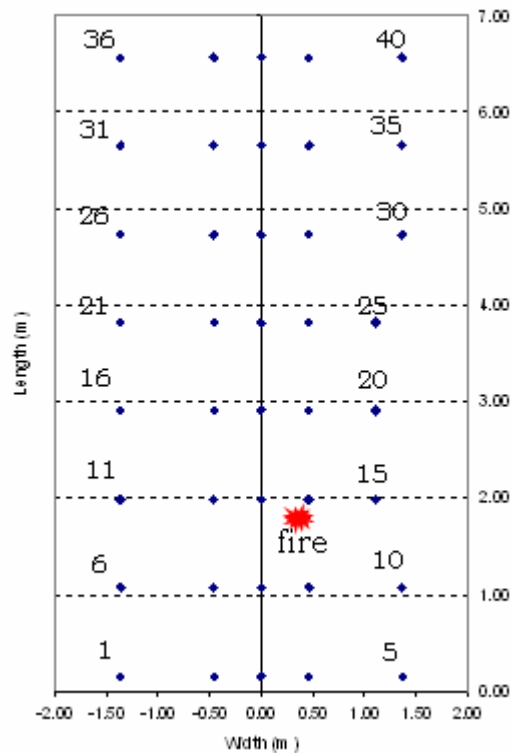


Figure 15. Instrumentation Schematic for Sidewall Scenario

Experimental temperatures for the attached flow sidewall configuration are shown in figure 16. The scatter plot shows the average temperature for each thermocouple at 60, 120, and 180

seconds and the uncertainty associated with the measurement. The error bars represent the 95% confidence interval, created using the experimental variation and the instrument drift (0.5 K).

The trends in the temperatures correspond roughly to the fire location. At all times, TC8, TC9, TC13, TC14, and TC15 record the highest temperatures since they are closest to the fire. One would expect TC14 to be the highest since it is closest to the fire, but instead, TC13 is the highest, although the experimental uncertainty bands for TC13 and TC14 overlap. The temperatures increase from 60 to 120 seconds, but they do not significantly increase at 180 seconds. The temperatures for this case are lower than for the baseline or the corner cases.

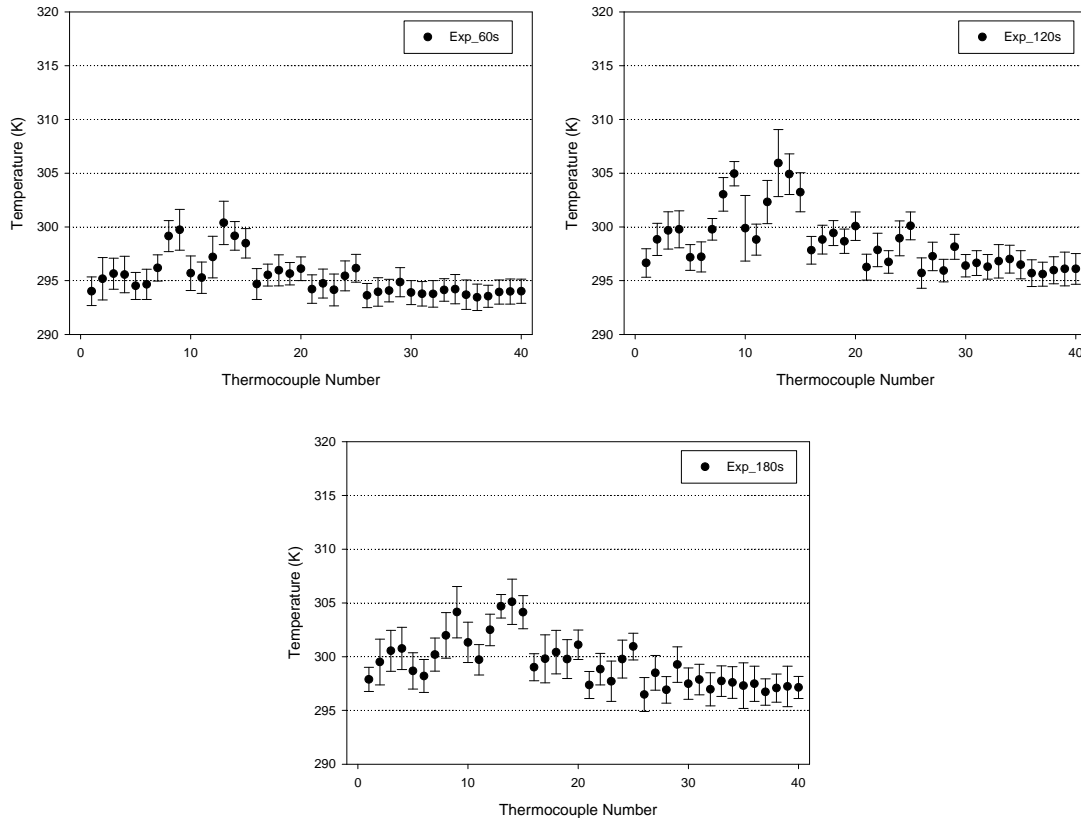


Figure 16. B-707 Sidewall Experimental Temperatures

8.1.2 Comparison of Experimental and Computational Temperatures.

The temperature comparisons for the sidewall scenario are shown in figure 17. At 60 seconds after ignition, the highest predicted temperatures occur at TC14, which is closest to the fire. The temperatures near the fire (TC14 and TC15) are slightly overpredicted at this early time. By 120 seconds after ignition, some of the temperatures in the vicinity of the fire are still slightly overpredicted. It is also interesting to note that now the highest temperatures are around the upper perimeter (i.e., thermocouples near the sidewalls, TC1-TC5, and TC10) indicating that perhaps there is a small amount of hot gases concentrating in those regions. This effect is not as pronounced in the experimental data. By 180 seconds after ignition, the agreement in both the trends and the magnitudes of the temperatures is good.

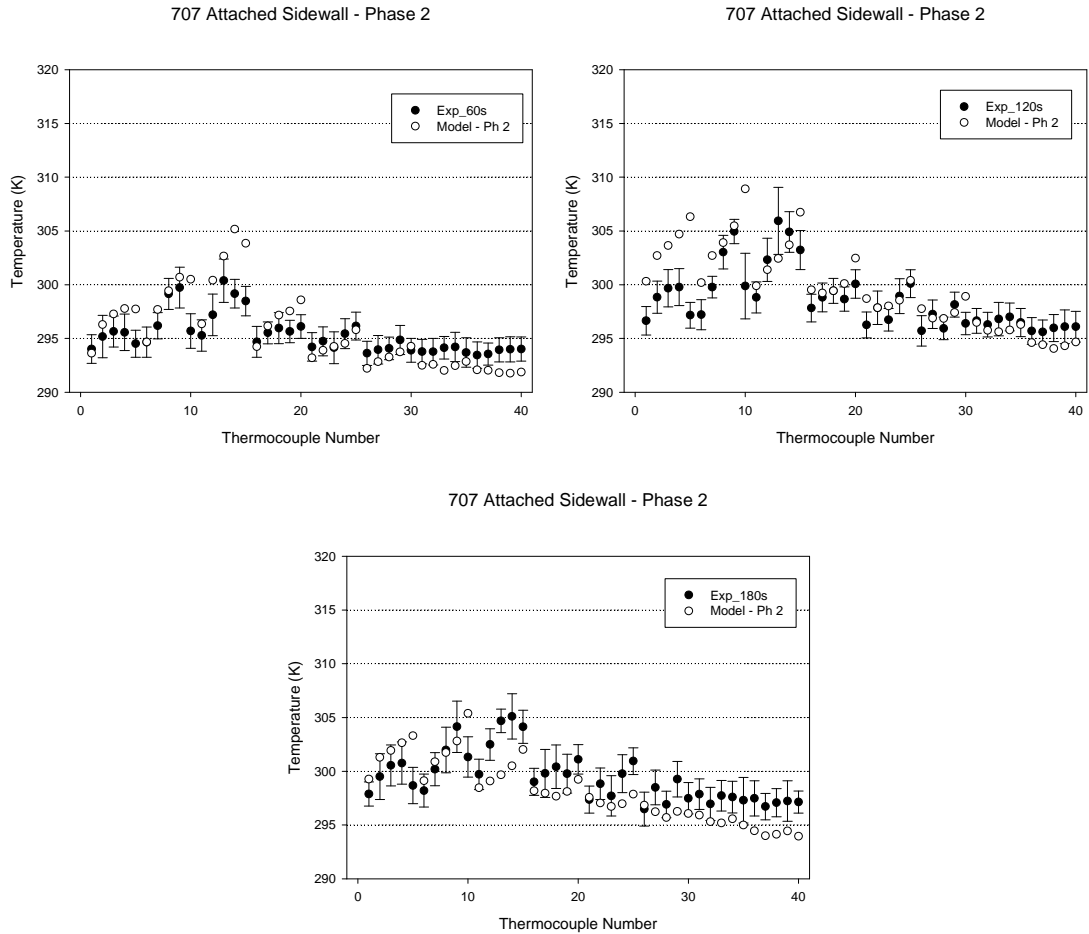


Figure 17. B-707 Sidewall Temperature Comparisons

8.2 LIGHT TRANSMISSION.

8.2.1 Experimental Light Transmission.

Experimental light transmission data for the attached flow sidewall configuration are shown in figure 18. The trends in the smokemeter readings are consistent with the fire location for the attached sidewall case. At 30 seconds after ignition, the forward meter has the greatest attenuation, followed by the mid meter. The aft meter and the three vertical meters are not attenuated since the smoke has not reached those locations in the short period of time. By 45 seconds, all three ceiling smokemeters are considerably attenuated, but the smoke has not started filling the compartment from the top to the bottom indicated by the vertical meters that are still near 100%. At 60 seconds after ignition, the three ceiling meters are below the 80% confidence threshold, while the vertical smokemeters are not indicating that smoke is present. By 120 seconds after ignition, only the lower two vertical smokemeters are measuring light transmission above the confidence threshold. In the final plot at 180 seconds after ignition, the lowest vertical smokemeter is at approximately 96% light transmission.

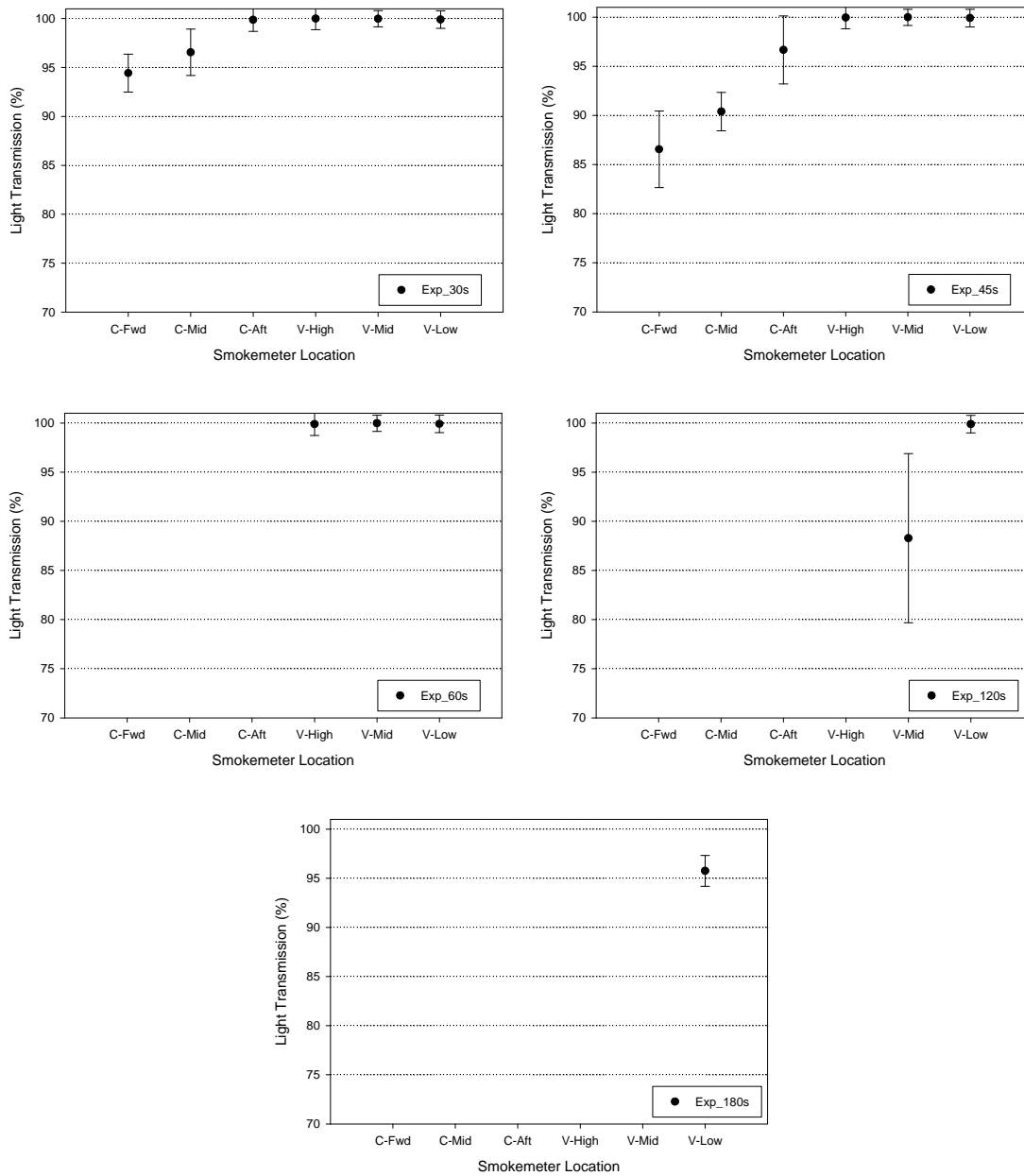


Figure 18. B-707 Sidewall Experimental Light Transmission

8.2.2 Comparison of Experimental and Computational Light Transmission.

Smokemeter validation comparisons for the sidewall scenario are shown in figure 19. Agreement in both the trends and magnitudes for the light transmission is good. The only discrepancy that occurs is for the low smokemeter at 120 and 180 seconds, which is well beyond the ideal detection time.

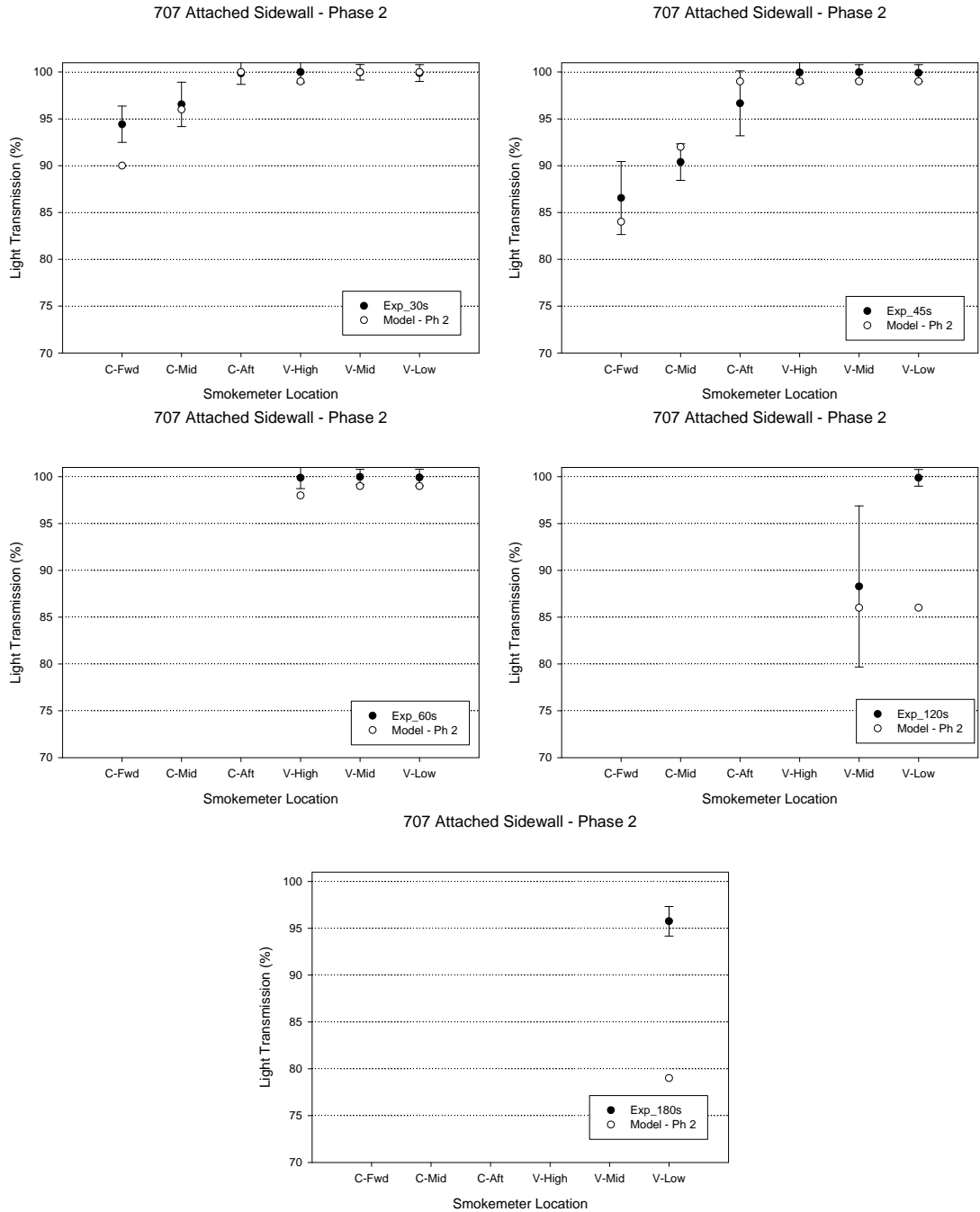


Figure 19. B-707 Sidewall Light Transmission Comparisons

8.3 GAS CONCENTRATIONS.

8.3.1 Experimental Gas Concentrations.

Experimental gas concentration data for the attached flow sidewall configuration are shown in figure 20. The results displayed are for the mid pan location at times of 60, 120, and 180 seconds after ignition. At 60 seconds after ignition the CO and CO₂ concentrations in the mid

pan are quite low. By 120 seconds, the concentrations increase significantly indicating that it takes some time for the levels to reach and build within the mid pan recessed areas. The concentrations then only slightly increase by 180 seconds after ignition, consistent with the observation that the smoke is now filling the rest of the compartment.

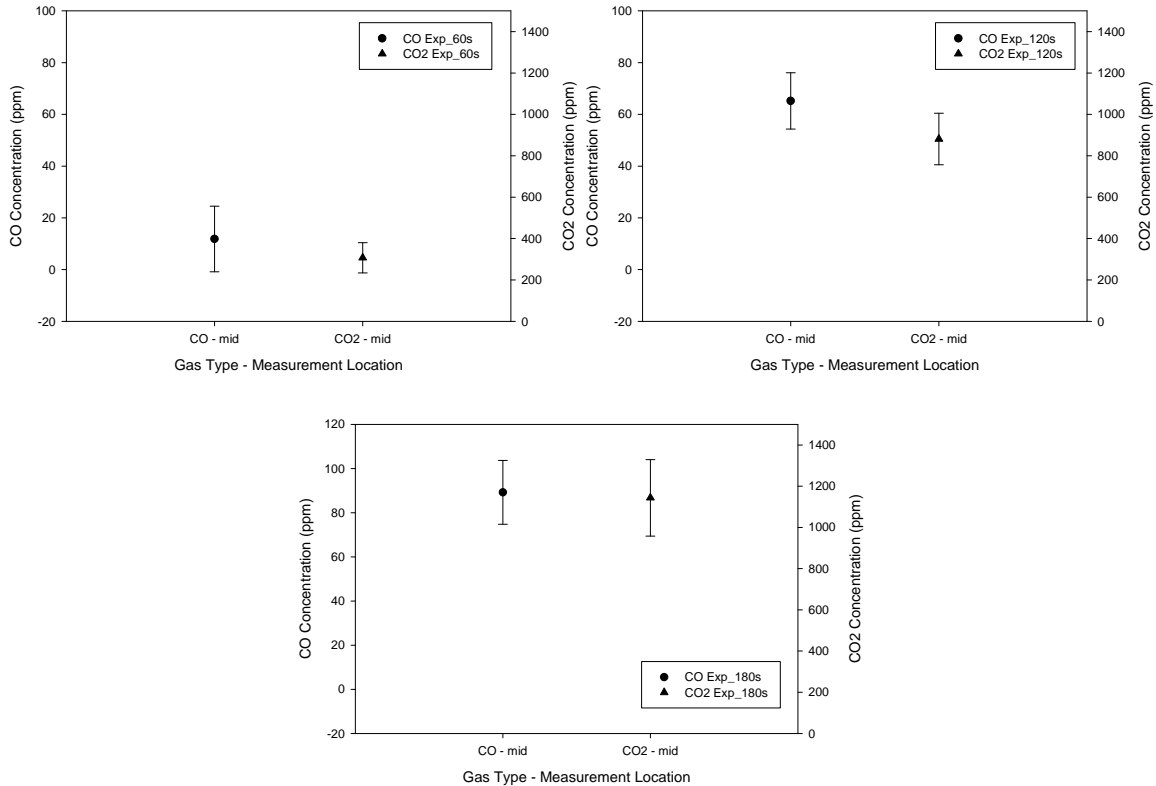


Figure 20. B-707 Attached Sidewall Experimental Gas Concentrations

8.3.2 Comparison of Experimental and Computational Gas Concentrations.

Validation comparisons for the sidewall gas concentrations are shown in figure 21. Agreement between the model predictions and the experimental measurements is favorable for all of the metrics. Some minor deviations from the experimental measurements are observed, but the predictions are still useful in providing insight into the transport of species within the compartment.

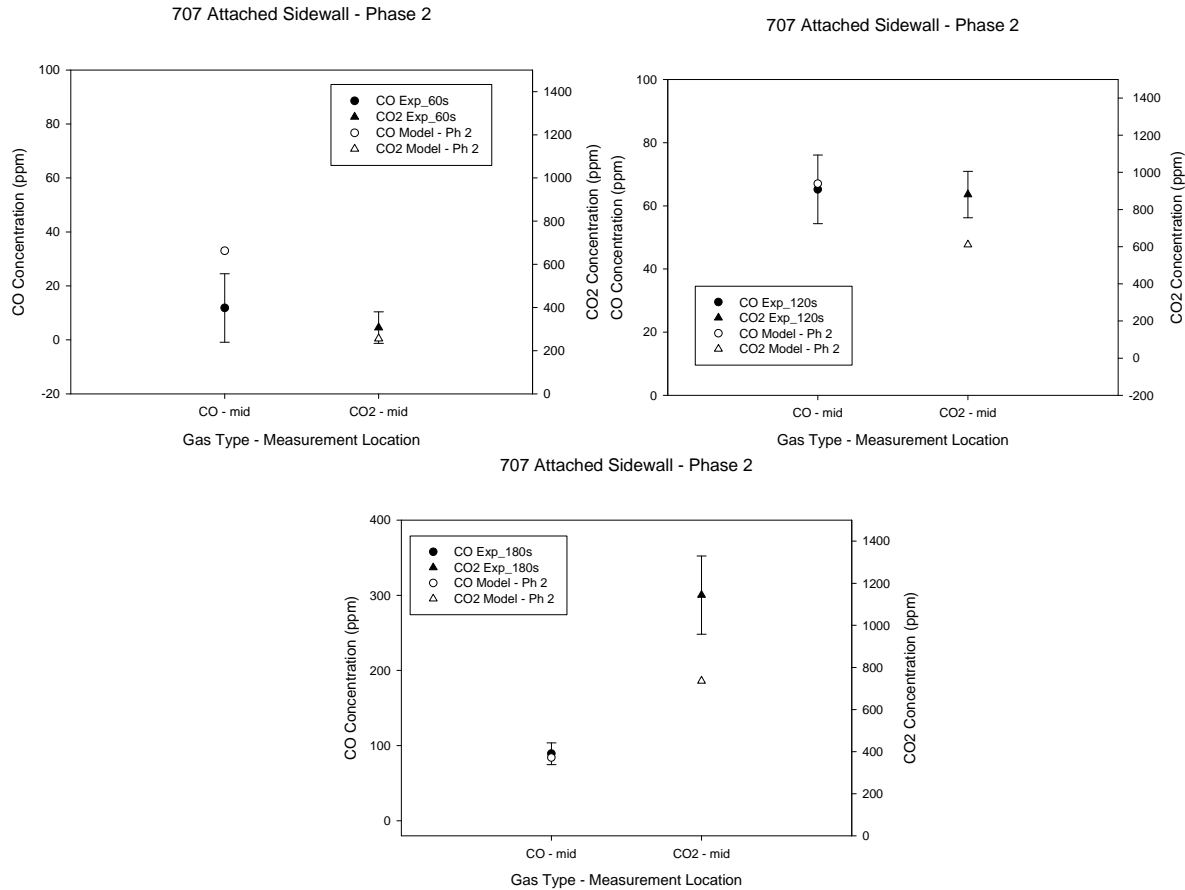


Figure 21. B-707 Sidewall Gas Concentration Comparisons

8.4 CONCLUSIONS FOR THE B-707 ATTACHED SIDEWALL CASE.

The predicted values for the light transmission and the gas concentrations were good for the attached sidewall case. Although the agreement in temperatures was not as good as the light transmission and gas concentrations, the code still does a reasonable job of indicating relative trends and magnitudes. The results indicate that the model's ability to predicted smoke transport in a cargo compartment is good even when the fire source is located near a sidewall. Thus, the model captures the dominant physics necessary to predict transport when there is a potential to interact with walls.

9. B-707 CORNER.

9.1 TEMPERATURES.

9.1.1 Experimental Temperatures.

To assist in the interpretation of the temperature measurements presented in this section, a schematic of the location of the thermocouples relative to the fire source is provided in figure 22.

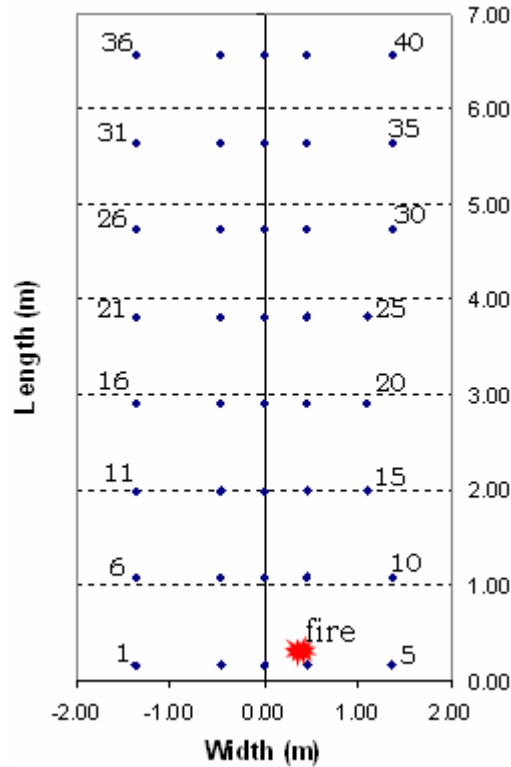


Figure 22. Instrumentation Schematic for Corner Scenario

Experimental temperatures for the attached flow corner configuration are shown in figure 23. The scatter plot shows the average temperature for each thermocouple at 60, 120, and 180 seconds and the uncertainty associated with the measurement. The error bars represent the 95% confidence interval, created using the experimental variation and the instrument drift (0.5 K).

Similar to the other two B-707 cases, the thermocouple temperature trends are consistent with the fire location (i.e., TC4 is closest to the fire). At 60 seconds after ignition, the maximum temperature is 308 K, but there is considerable variability in this likely due to the variability in the initial burning phase of the fire source. By 120 seconds, the maximum temperature increased to 315 K with much less uncertainty. At the final measurement time, 180 seconds, the maximum temperature has decreased to 310 K. The maximum temperatures recorded are similar to the baseline experiments, which are higher than the sidewall scenario. These higher temperatures could potentially be caused by the thermocouples location relative to a recirculation zone in the corner region.

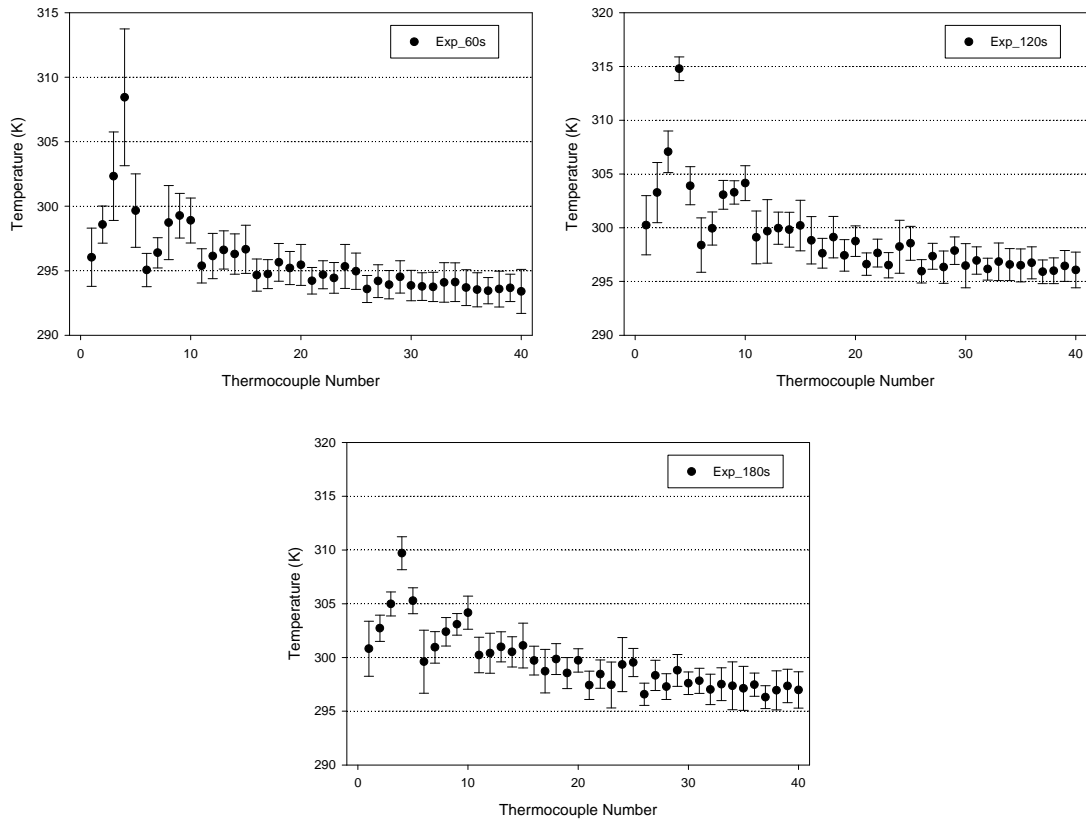


Figure 23. B-707 Corner Experimental Temperatures

9.1.2 Comparison of Experimental and Computational Temperatures.

Comparisons of the temperature validation metrics for the corner scenario are shown in figure 24. At 60 seconds after ignition, there is very good agreement in the temperatures except for TC5, TC10, and TC15. These thermocouples are located along the edge of the ceiling in the region surrounding the fire source. A similar increase in predicted temperatures for thermocouples in this region was also seen in the sidewall scenario. Similarly, at 120 seconds after ignition, the most significant differences between the predictions and the experiments are observed for thermocouples along this edge of the ceiling. Otherwise, the trends and magnitudes are similar. The agreement at 180 seconds after ignition is better than at the earlier times.

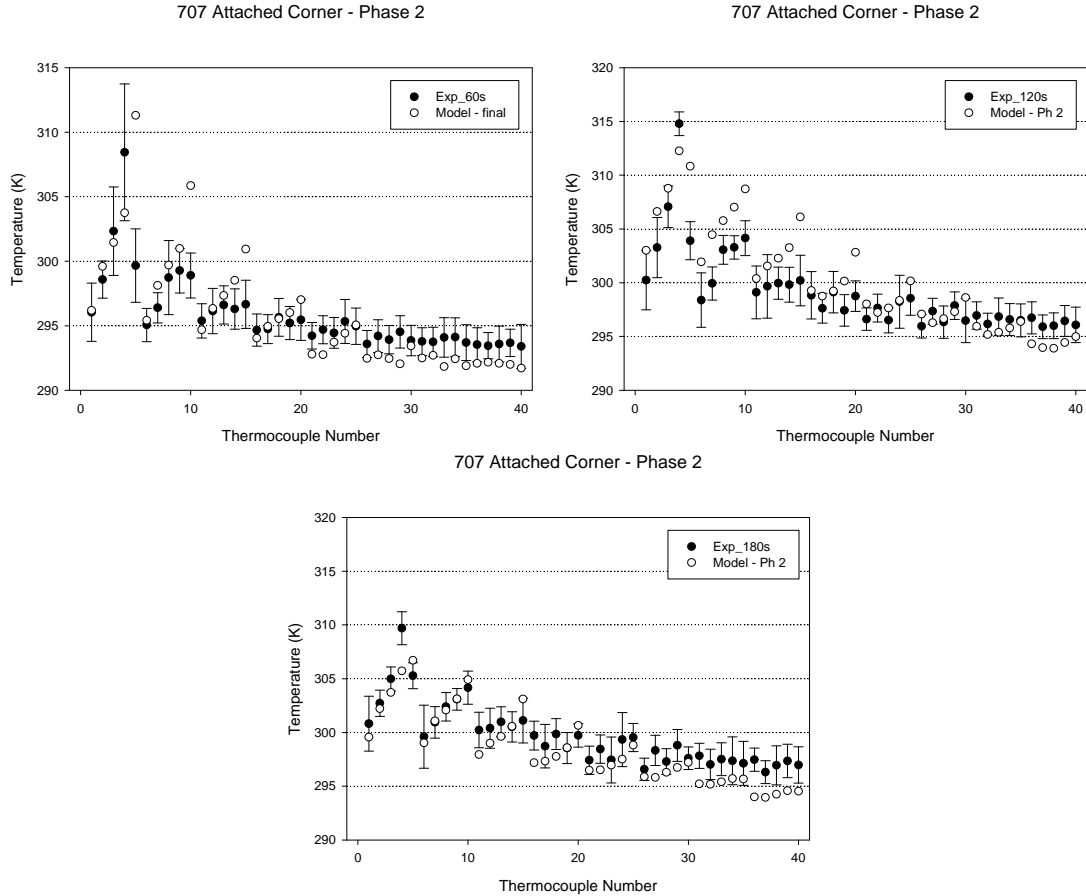


Figure 24. Corner B-707 Comparison of Temperatures

9.2 LIGHT TRANSMISSION.

9.2.1 Experimental Light Transmission.

Experimental light transmission data for the attached flow corner configuration are shown in figure 25. The data obtained from the smokemeters in the corner configuration are consistent with the fire location. For example, the forward (fwd) smokemeter responds first, followed by the mid smokemeter, and then the aft smokemeter. The mid and aft smokemeters record the presence of smoke more slowly than in the sidewall case since the fire is located farther forward in the compartment in the corner scenario. Similar to the sidewall case, the middle vertical smokemeter reading has considerable uncertainty at 180 seconds after ignition.

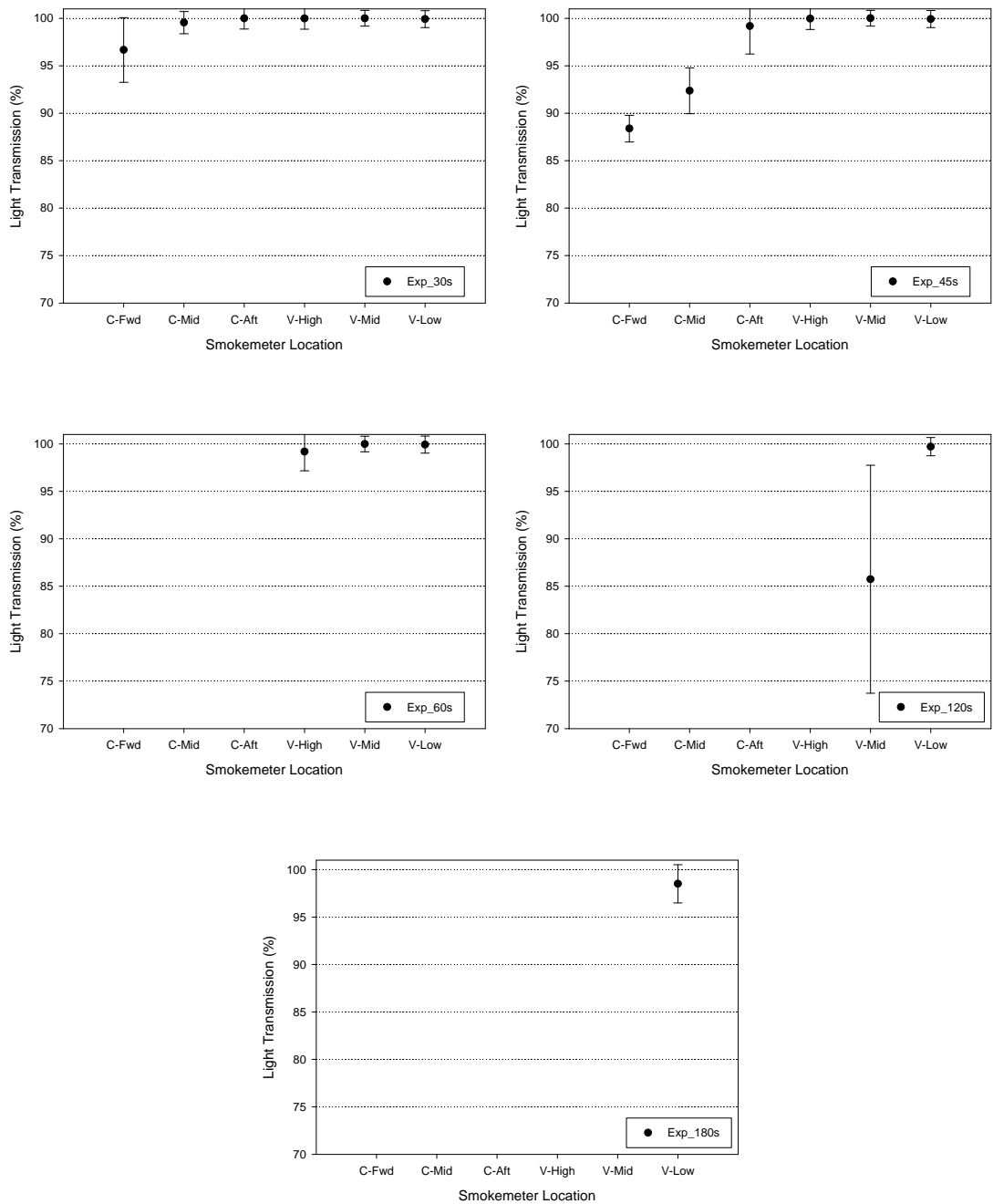


Figure 25. B-707 Attached Corner Experimental Light Transmission

9.2.2 Comparison of Experimental and Computational Light Transmission.

Comparisons of the light transmission validation metrics are shown in figure 26. Overall, there is excellent agreement between the predictions and the experimental measurements. The only deviation occurs at late times (120 and 180 seconds) for the low smokemeter. This is not seen as significant since detection is required at an earlier time and it is anticipated that all detection

systems will be located higher in the compartment to take advantage of the expected rise of the hot combustion products.

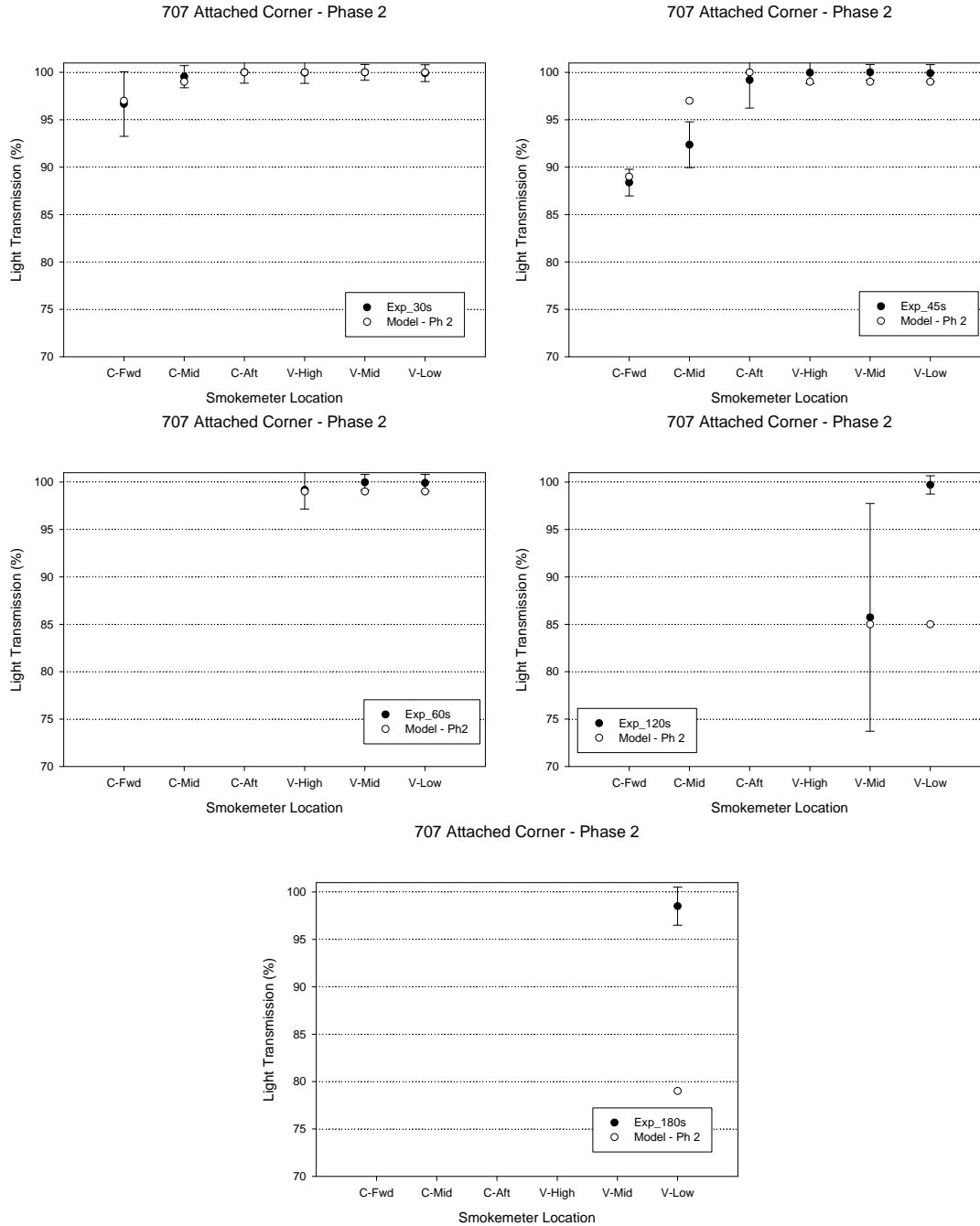


Figure 26. B-707 Attached Corner Comparison of Light Transmission

9.3 GAS CONCENTRATIONS.

9.3.1 Experimental Gas Concentrations.

Experimental gas concentration data for the attached flow sidewall configuration are shown in figure 27. The gas concentration results for the corner configuration are similar to the sidewall configuration. The recorded levels are low at 60 seconds, but they increase significantly by 120 second. Then, from 120 seconds to 180 seconds, there appears to be little change. Overall, compartment trends could be observed if data were available for the aft and TC36 locations as they were in the baseline case, but the data presented here will be sufficient for model validation.

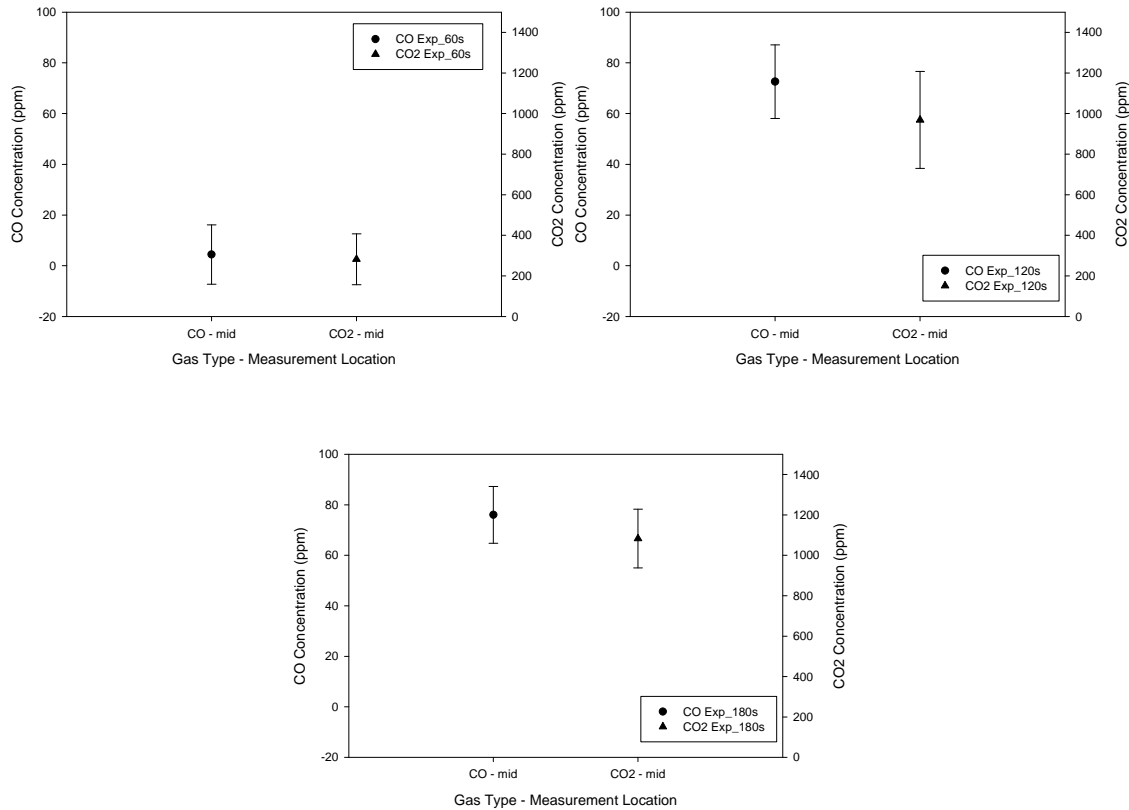


Figure 27. B-707 Attached Corner Experimental Gas Concentrations

9.3.2 Comparison of Experimental and Computational Gas Concentrations.

The comparisons of the gas concentrations for the attached corner case are shown in figure 28. The agreement between the predictions and the experimental measurements for most of the metrics is good.

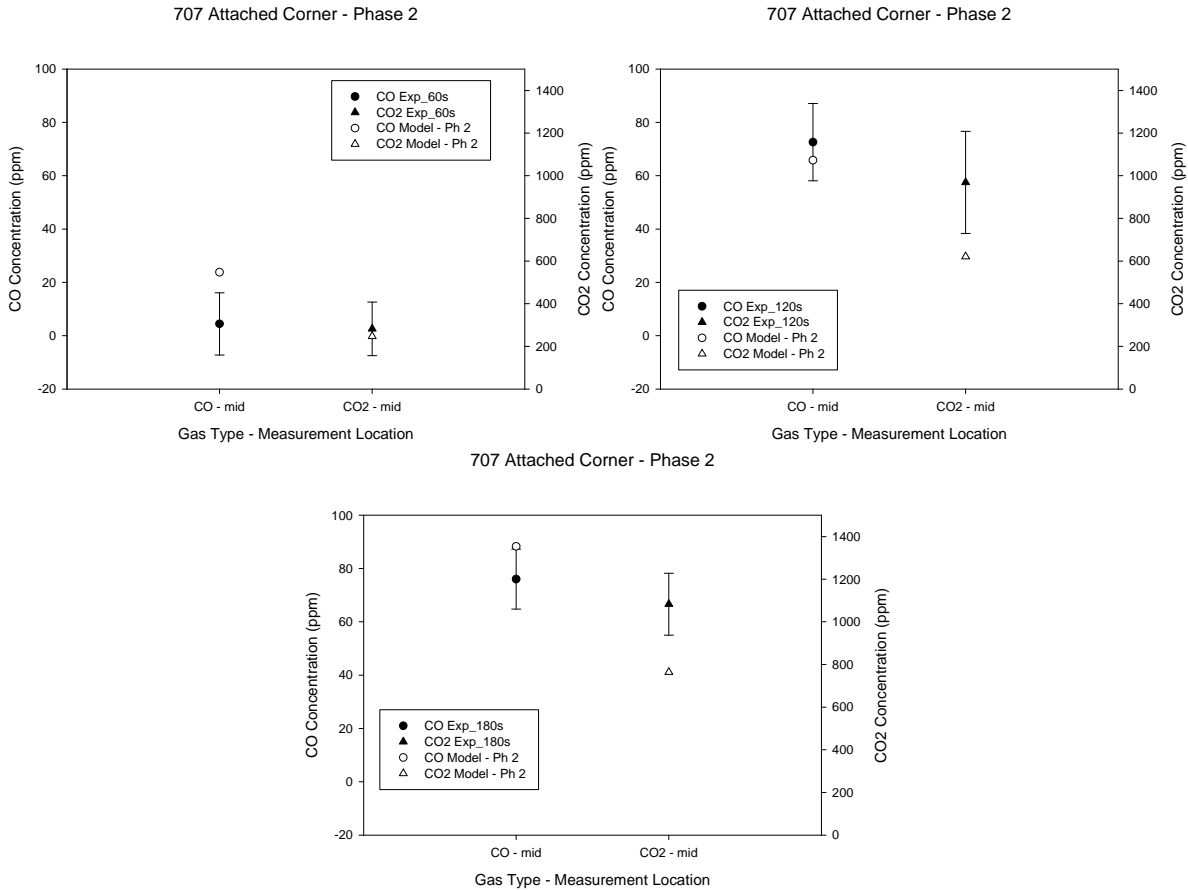


Figure 28. B-707 Attached Corner Comparison of Gas Concentrations

9.4 CONCLUSIONS FOR THE B-707 ATTACHED CORNER SCENARIO.

The comparisons of all validation metrics for the corner scenario were presented in sections 9.1 through 9.3. The agreement between the code prediction and the experimental measurements was very good for the smokemeters and the gas concentrations. The agreement in the temperature was adequate. Overall, the model should provide good prediction of the smoke transport in a cargo compartment for a fire located in or near a corner region.

10. DC-10 BASELINE.

10.1 TEMPERATURES.

10.1.1 Experimental Temperatures.

The DC-10 baseline scenario temperatures are presented in the following section. A schematic of the thermocouple locations relative to the fire location is shown in figure 29 to assist in the interpretation of the observed trends. Experimental temperatures for the thermocouples in the DC-10 baseline case are shown in figure 30 for 60, 120, and 180 seconds after ignition. For all times and measurement locations, the temperature rise is almost negligible. It is evident that the size of the compartment and the ventilation has greatly impacted the temperature rises. In all

B-707 cases, the temperature rises were measurable and significant. It appears that a larger fire or less ventilation would be required to result in measurable temperature rises. Comparison of the code to the experimental results for this case will evidently be more meaningful for the other selected metrics.

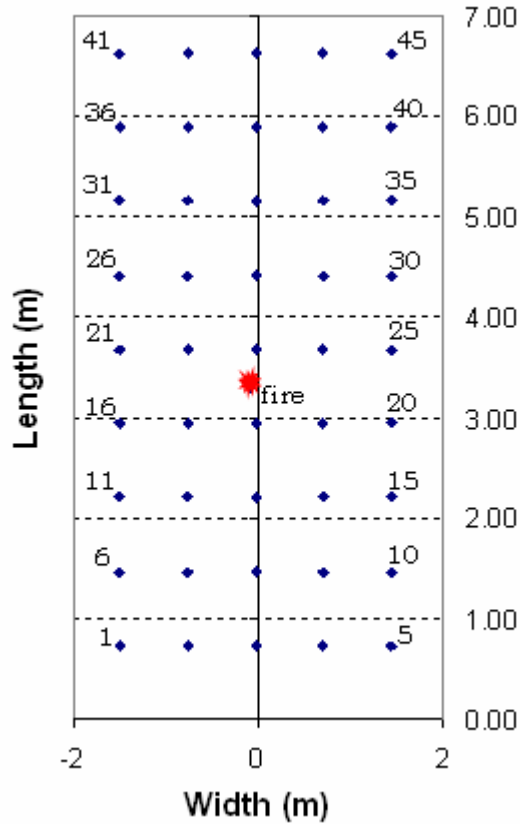


Figure 29. Schematic of DC-10 Thermocouples and Fire Location

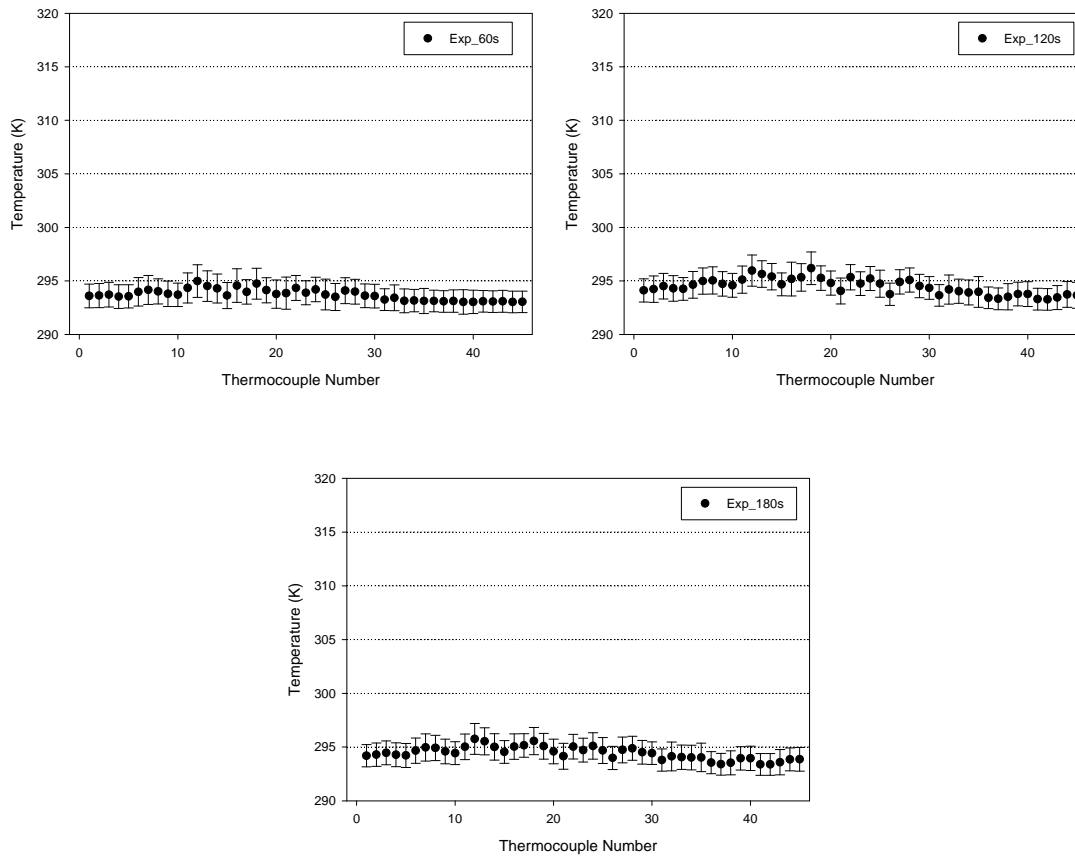


Figure 30. DC-10 Baseline Experimental Temperatures at 60, 120, and 180 Seconds

10.1.2 Comparison of Experimental and Computational Temperatures.

The comparison of experimental and computational temperatures for the DC-10 configuration is shown in figure 31. Most of the predicted temperatures fall within the experimental uncertainty bands except for a few thermocouples near the fire. The temperature of these thermocouples is higher than the experimental temperatures by a few degrees.

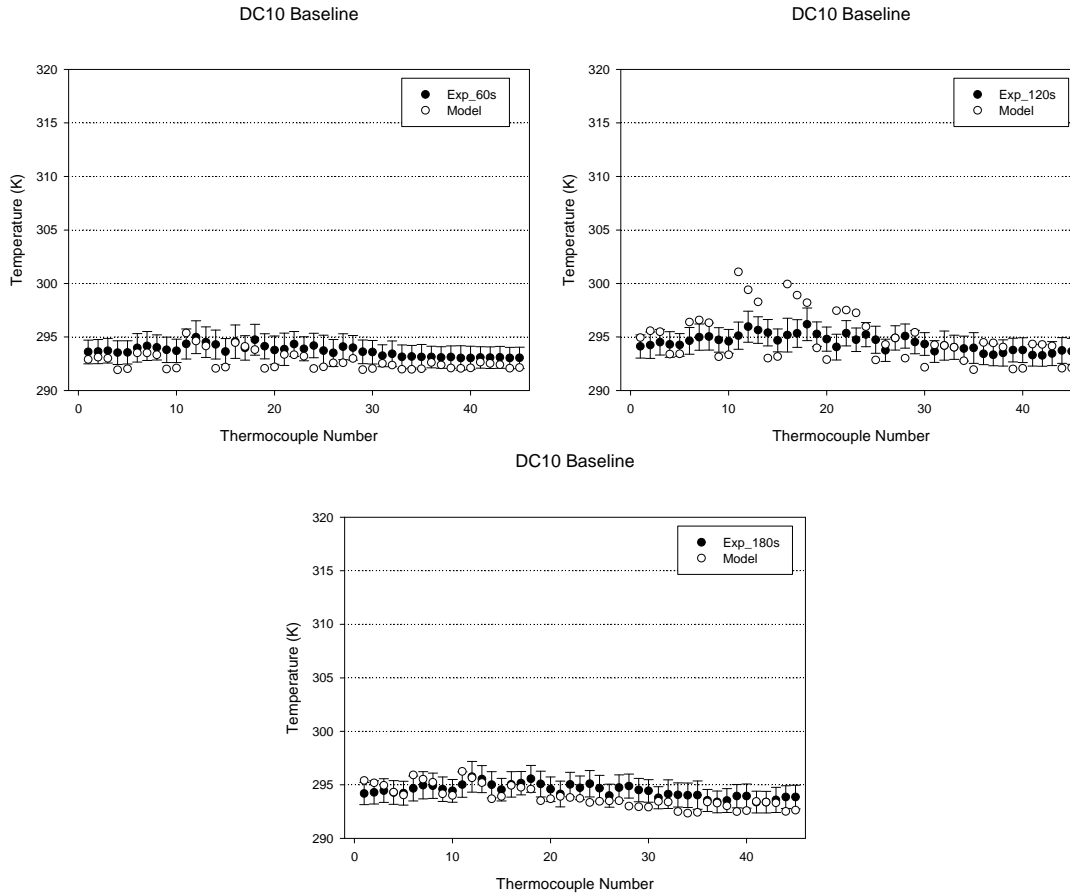


Figure 31. DC-10 Baseline Comparison of Temperatures

10.2 LIGHT TRANSMISSION.

10.2.1 Experimental Light Transmission.

Experimental light transmission measurement results are shown in figure 32 for times after ignition of 30, 45, 60, 90, 120, and 180 seconds. Measurements in this compartment were made at locations designated forward, mid, aft, and 5' (centered about the forward recessed area) as documented in figure 3. The observed trends are reasonable given the location of the fire. As expected, the 5' smokemeter with the smallest path length responds to the smoke first as seen in the 30-second plot. It is also important to note that, overall, the measurements made by this smokemeter have a considerable amount of variability. At 45 and 60 seconds after ignition, both the 5' and the forward smokemeters are impacted by the smoke in the compartment, while the other two (mid and aft) are still at 100% light transmission. The mid smokemeter decreases a few percent by 90 seconds after ignition, and the light transmission continues to decrease at 120 and 180 seconds after ignition. At 180 seconds after ignition, the aft smokemeter finally begins to sense the smoke.

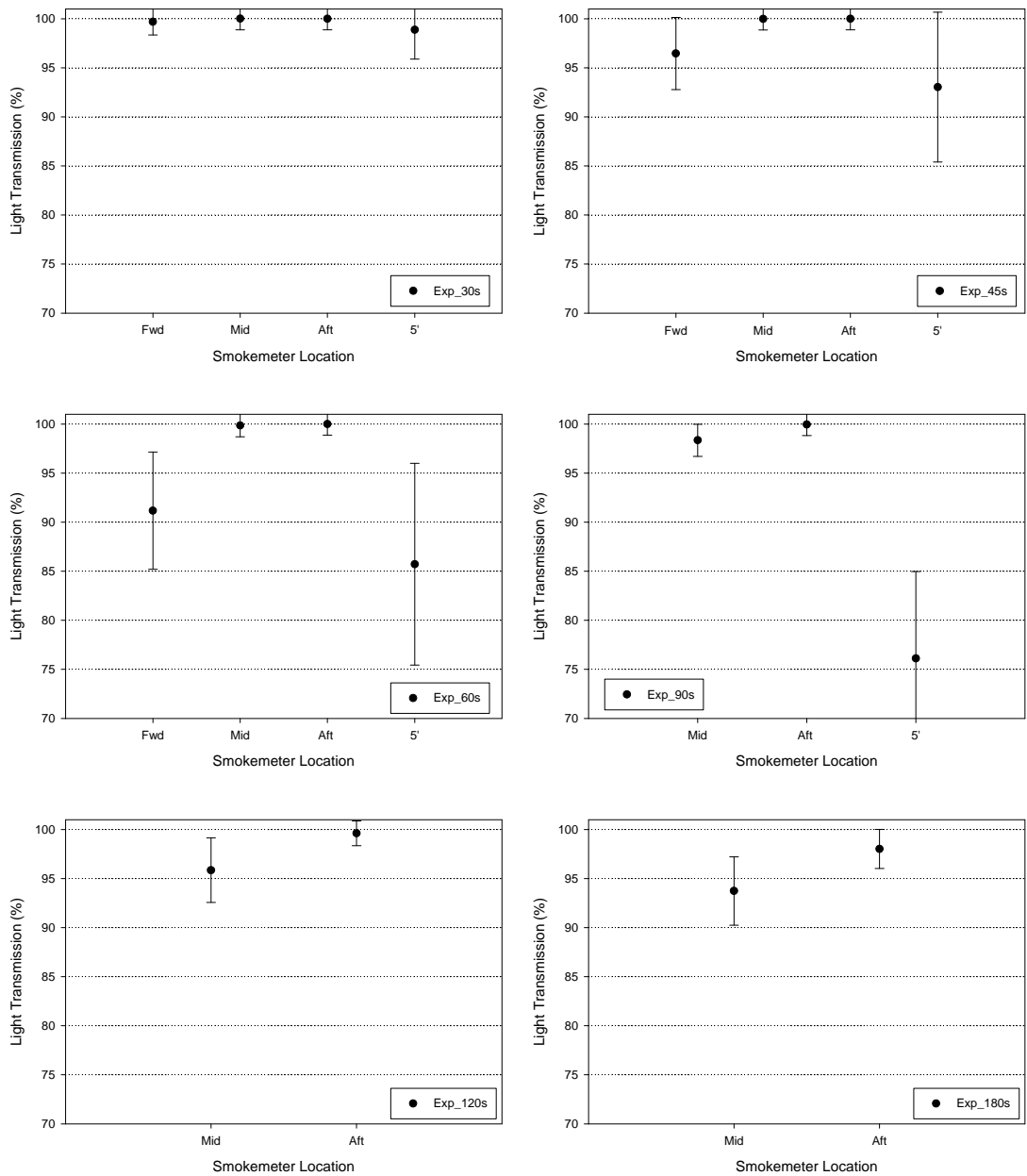


Figure 32. DC-10 Baseline Experimental Light Transmission

10.2.2 Comparison of Experimental and Computational Light Transmission.

The comparisons of the light transmission metrics for the DC-10 case are shown in figure 33. The agreement between the predictions and the experimental measurements is excellent. The only time the predictions fall outside the experimental uncertainty band (5% high) is for the 5' smokemeter at 90 seconds after ignition, but this experimental measurement is nearing the threshold of use since the uncertainty increases greatly at this level. For all other times and locations, the predictions are well within the experimental uncertainty bands.

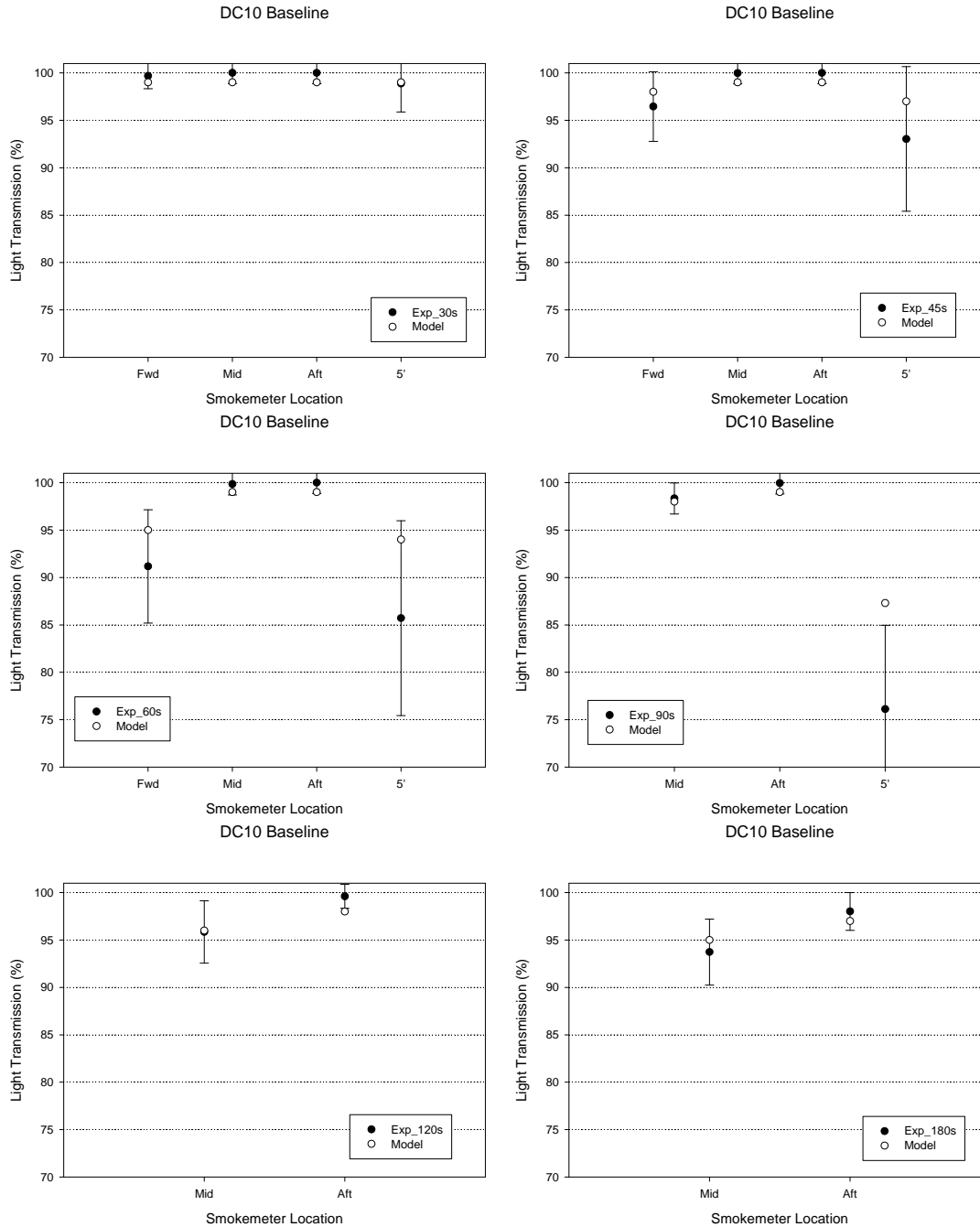


Figure 33. DC-10 Baseline Comparison of Experimental and Computational Light Transmission

10.3 GAS CONCENTRATIONS.

10.3.1 Experimental Gas Concentrations.

Experimental gas concentration data for the DC-10 baseline configuration are shown in figure 34 for 60, 120, and 180 seconds after ignition. The measurement locations are in the forward recessed area, aft recessed area, and near thermocouple 5. The observed trends are reasonable

given the location of the fire (i.e., forward responds first, followed by TC5, and then the aft location). Concentrations of CO and CO₂ at the measurement locations increase from 60 to 120 seconds after ignition, but then they are relatively stable from 120 to 180 seconds. The measured maximum CO and CO₂ concentrations for the DC-10 baseline scenario are considerably lower (approximately two times) than any B-707 configuration measurements.

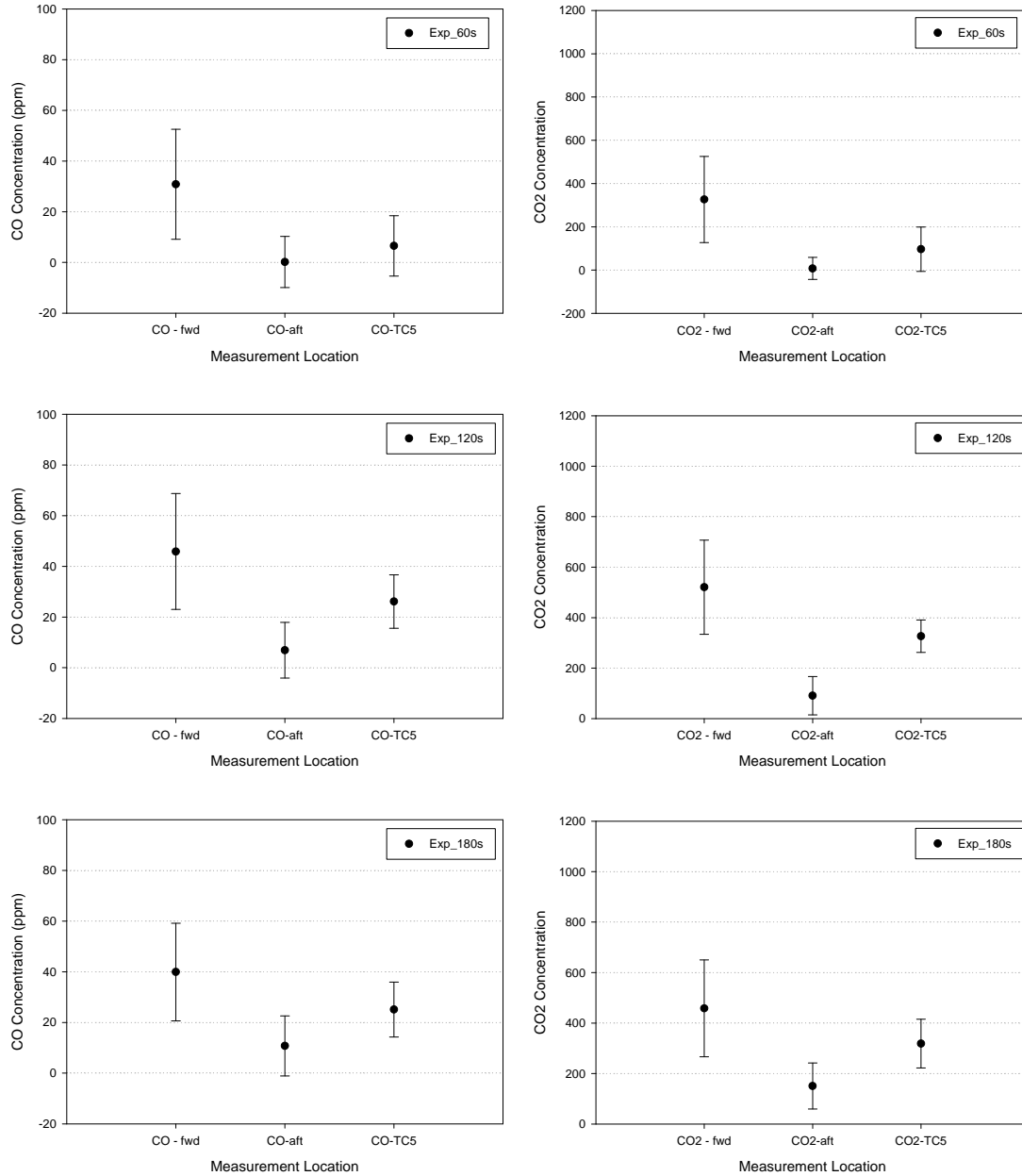


Figure 34. DC-10 Baseline Experimental Gas Concentrations

10.3.2 Comparison of Experimental and Computational Gas Concentrations.

The comparison of the gas concentration predictions and measurements are shown in figure 35. The model does an excellent job of predicting the concentrations of CO and CO₂ for this large compartment with significant forced ventilation.

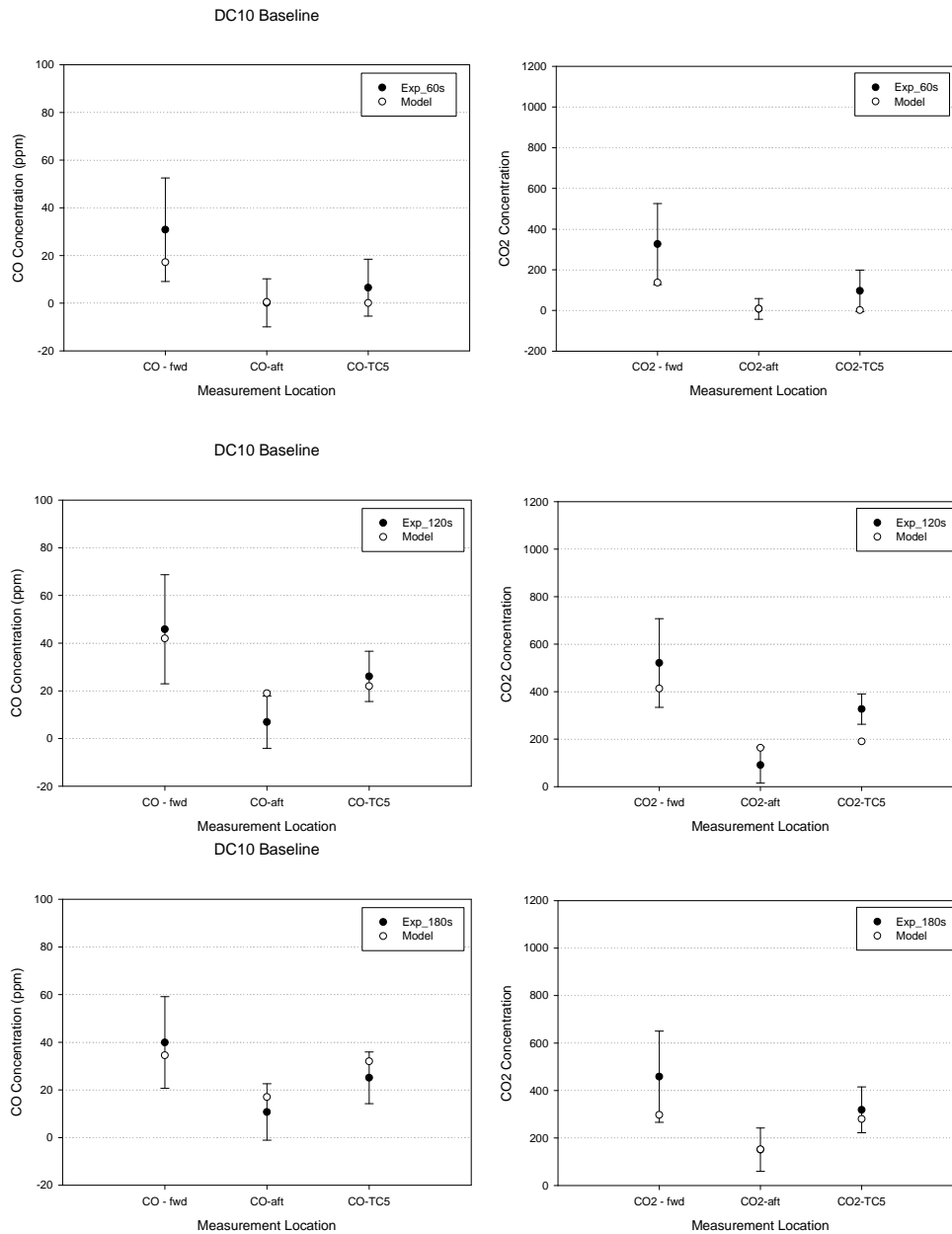


Figure 35. DC-10 Comparison of Experimental and Computational Gas Concentrations

10.4 CONCLUSIONS FOR THE DC-10 BASELINE SCENARIO.

The previous section presented the results for the comparison of the validation metrics for the DC-10 scenario. This scenario was intended to test the ability of the model to predict the transport of fire products within a wide-body aircraft with forced air ventilation. The same fire source that was used in the B-707 experiments was also used in the DC-10 experiments. This fire source was relatively small for such a large compartment with forced ventilation, which resulted in negligible temperature rise. The computational model also predicted negligible temperature rise, except at a few thermocouples near the fire source. The computational model predicted the light transmission and gas concentrations very well. Overall, the comparisons provide confidence in the models ability to predict the transport of combustion products within a well ventilated wide-body aircraft.

11. TRANSPORT CODE VARIABLES.

11.1 GRID.

A grid sensitivity study was performed for the DC-10 scenario. The grid size was reduced by a factor of two near the door for approximately 1/3 the distance of the compartment. The grid size was also reduced in the y-direction near the inlets for about 1/2 the distance of the compartment. This required a reduction in the time step from 0.01 to 0.005, and increased the run time of the simulation to approximately 2 days. This change in the grid did not cause a significant difference in the results.

An additional grid sensitivity study was performed for the B-707 compartment. The simulations were run using grids that were 5 by 5 by 10 (coarse), 10 by 10 by 20 (medium), and 20 by 20 by 40 (fine) cells. In addition, refinement of the coarse and medium grids near the vicinity of the fire was performed to produce a fire with the same area as the fine grid. Overall, the results from five different cases were compared. The results did not differ by more than 3% for temperature and light transmission. The greatest difference was seen near the fire source, as expected. At thermocouples away from the fire source, typically the difference was less than 1%.

11.2 FIRE LOCATION.

To assess the sensitivity of the results to fire location, two slightly different runs were performed for the sidewall scenario. The x location (width) of the fire was moved from 0.41 to 0.54 m. The experimental fire location was at 0.43 m. The small modification of the fire location did not change the results significantly. Figure 36 shows the example plots displaying the minimal change that resulted with the alteration of the fire location.

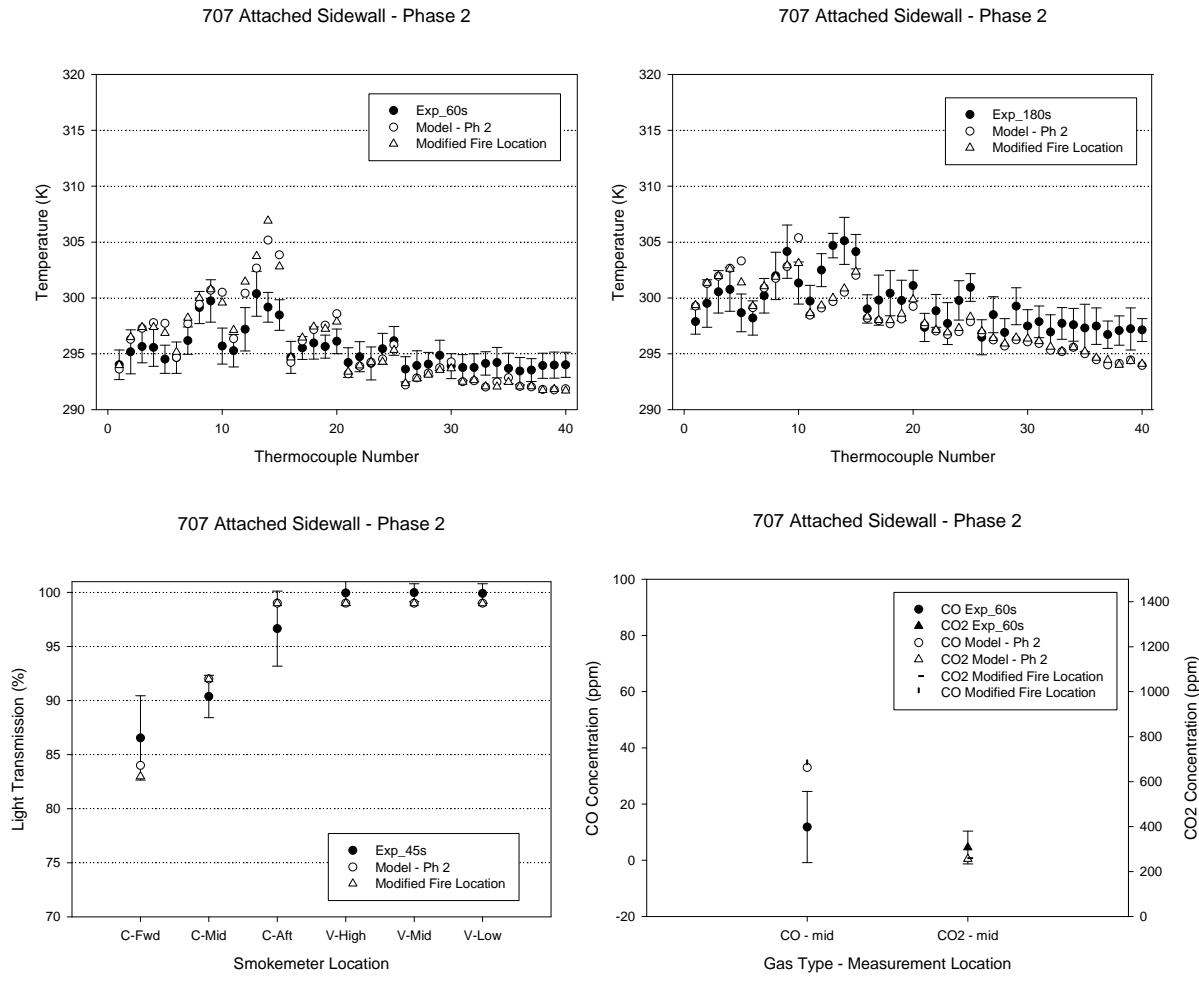


Figure 36. Comparison of Results With Modified Fire Location

11.3 HEAT TRANSFER COEFFICIENT

Initial comparisons of the temperatures predicted by the model were unsatisfactory in the phase 1 validation. Modifications to both the model and experiments were initiated prior to the phase 2 comparisons. The addition of a heat transfer subroutine to account for the heat loss to the cargo compartment walls was one of the modifications to the code that occurred.

The baseline B-707 simulations used a heat transfer coefficient of $7 \text{ W/m}^2\text{K}$. To assess the sensitivity of the simulations to the coefficient, the results are compared to simulations with varying heat transfer coefficients (0 and $14 \text{ W/m}^2\text{K}$). The results are shown in figure 37. The simulation with no heat transfer to the walls results in temperatures that are significantly higher than the experiments and the other simulations. This provides evidence that the heat transfer subroutine was a necessary addition. There is some difference between the $h = 7 \text{ W/m}^2\text{K}$ (baseline) and the $h = 14 \text{ W/m}^2\text{K}$ simulations, but it is not as significant.

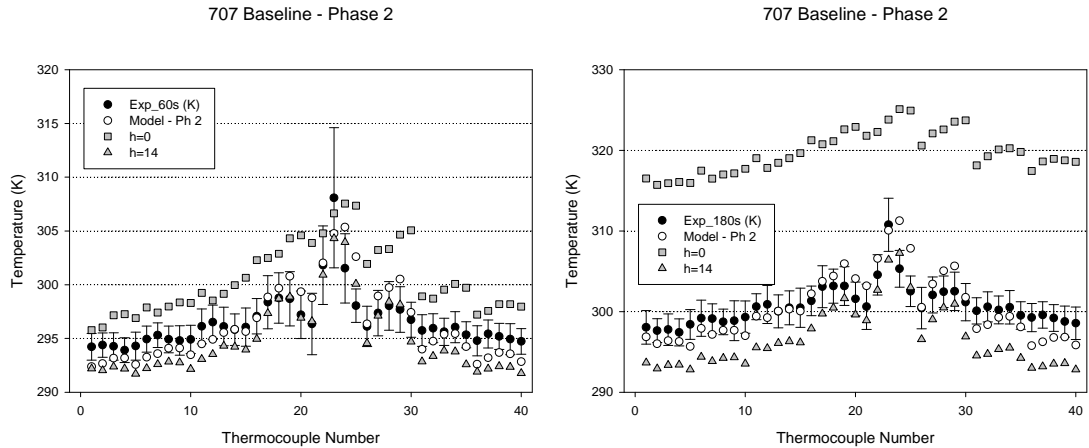


Figure 37. Comparison of B-707 Simulation With Different Heat Transfer Coefficients (60 and 120 Seconds)

In one DC-10 simulation, the heat transfer coefficient was increased by a factor of two (from 7 W/m²K to 14 W/m²K). There was a negligible change in the results due to this increase. The minimal change was expected since the gas temperatures within the DC-10 compartment were very low due to the high ventilation rate. The low gas temperatures would result in minimal heat loss to the walls since the temperature differential between the walls and the gas was very small.

11.4 TIME STEP SELECTION.

There is a condition of concern that could be encountered while running the model. If the velocities in certain regions are very high, a large time step will cause instability in the simulation. Although there are several criteria for selecting a time step in any case, the time step selected should not exceed the cell length divided by the maximum velocity in that cell neighborhood.

One location of high velocity is near the ceiling directly over the fire. An estimate of the velocity at this location can be had from reference 4

$$U = 0.96 \cdot \left[\frac{Q}{H} \right]^{\frac{1}{3}} \text{ m/s}$$

where Q is the fire heat release rate (3 kW) and H is the compartment height in meters.

For ventilated compartments, the area directly above the fire is not the only location of a high velocity. Another region was observed near the door region of the DC-10. The small cell size at the exit resulted in high velocities, ultimately leading to failure of the simulation at 180 seconds. Modification of the grid in the door region resolved the issue. If careful attention is given to the maximum velocity and cell size when selecting the time step, this issue should not arise.

If an appropriate time step is selected, the code will diverge and not produce any results. The transport code is available to the public through a web site maintained by Sandia National

Laboratories. The web site also contains a Frequently Asked Question (FAQ) section and a tutorial for running the code. More detailed information on selecting an appropriate time step is contained in those two sections.

12. CERTIFICATION INSIGHT.

This section provides insight into certification simulations and experiments that were gained as a result of running the few simulations presented in this report. It is evident that much more could be learned if the computational tool was used to simulate and compare more certification scenarios.

The two different compartments and ventilation types (DC-10 versus B-707) resulted in very different experimental results. The magnitudes of the validation metrics were drastically impacted by the change in compartment size and ventilation. If detection is required in both compartments within the same time, a larger fire or a more sensitive detector will likely be needed in the larger, ventilated compartment. Temperature rise in the DC-10 compartment was negligible for the entire experiment. A detection system may be more successful in detecting a fire in this compartment if it alarmed based upon light transmission or gas concentration, although these signals would also be fairly weak. It is also evident that certification tests within such an aircraft would benefit from a larger fire source. The model could be used to determine the size of fire that would produce combustion products at a level that could be detected within the required alarm time.

Leakage ventilation flows in a narrow-body aircraft (~18 ft³/min) did not impact the results. Forced ventilation, similar to what existed in the DC-10, will impact the results. This type of ventilation should be characterized so that it might be used as a boundary condition in the simulations.

There was some indication that a concentration of heat and gases existed near the edges of the compartment, indicating that this region could be considered for placement of a smoke detector. More simulations could confirm or deny this possibility.

13. CONCLUSIONS.

A validated smoke transport model could be used to enhance the smoke detection system certification process by identifying worst-case locations for fires, optimum placement of fire detector sensors within the cargo compartment, and sensor alarm levels needed to achieve detection within the required certification time. This report presented the validation of such a model. Overall, the model favorably predicted the validation metrics for the selected cases. The spectrum of scenarios provided confidence in the models' ability to predict the transport of smoke and combustion products in a variety of conditions. The main variables that changed between the cases were fire location, compartment size, and ventilation. The model predicted the trends and magnitudes of the validation metrics as the simulation parameters changed. The model can now be used to simulate certification scenarios of interest to assist in designing the optimum detection systems for cargo compartments.

14. REFERENCES.

1. Suo-Anttila, J.M., Gill, W., Gallegos, C., and Nelsen, J. "Computational Fluid Dynamics Code for Smoke Transport During an Aircraft Cargo Compartment Fire: Transport Solver, Graphical User Interface, and Preliminary Baseline Validation," FAA report DOT/FAA/AR-03/49, October 2003.
2. Domino, S.P. and Voth, T.E., "Manufactured Solution Verification of FAA Smoke Transport Code," internal report to David Blake, March 2002.
3. Filipczak, R.A., Blake, D., Speitel, L., Lyon, R.E., Suo-Anttila, J.M., and Gill, W., "Development and Testing of a Smoke Generation Source," *Proceedings from the Fire and Materials Conference*, SAND2001-0151C, San Francisco, CA, 2001.
4. Coleman, H.W. and Steele, W.G., "Experimentation and Uncertainty Analysis for Engineers," John Wiley and Sons, New York, 1999.

APPENDIX A—MANUFACTURED SOLUTION VERIFICATION OF FEDERAL AVIATION ADMINISTRATION SMOKE TRANSPORT CODE

A.1 NOMENCLATURE.

CFL	Courant-Friedrichs-Lewy Number ($= U_0 \Delta t / \Delta x$)
$S_{mom,i}$	Source term for the x_i - momentum equation
t	time
u, u_1	x-velocity component
v, u_2	y-velocity component
w, u_3	z-velocity component
U_0	velocity amplitude/peak
x, x_1	x coordinate
y, x_2	y coordinate
z, x_3	z coordinate greek
Δt	time step
Δx	spatial discretization
ρ	density
μ	viscosity

A.2 INTRODUCTION.

This appendix documents the current manufactured solution verification status of the Federal Aviation Administration (FAA) code developed to model smoke transport in airplane cargo bays. A manufactured solution is devised and incorporated into the FAA smoke transport code. As the chosen manufactured solutions are not generally solutions to the Navier Stokes equations, source terms are added to the continuity and momentum equations to ensure consistency between solution and the partial differential equation.

The results presented here are intended to provide confidence that FAA smoke transport code has been coded correctly. Portions of the code that are touched by the test cases and result in accurate solutions may be considered verified. It is crucial to note that only those pieces that are exercised by these test problems may be considered verified. More details concerning the development and use of manufactured solutions may be found in Salari and Knupp (2000).

A.3 NAVIER STOKES EQUATIONS.

This section introduces the momentum and continuity equations as they are implemented in the FAA code. The momentum equations are assumed to have the form,

$$\frac{\partial(\rho u_i)}{\partial t} + \frac{\partial}{\partial x_j}(\rho u_i u_j) = -\frac{\partial P}{\partial x_i} + \frac{\partial}{\partial x_j} \left\{ \mu \left(\frac{\partial u_i}{\partial x_j} + \frac{\partial u_j}{\partial x_i} \right) \right\} + S_{mom,i}. \quad (A-1)$$

The continuity equation has the form,

$$\frac{\partial \rho}{\partial t} + \frac{\partial(\rho u_i)}{\partial x_i} = S_{cont} \quad (A-2)$$

A.4 SOURCE TERMS.

This section introduces the momentum and continuity source terms that are required so that the manufactured solution,

$$\begin{aligned} u(\mathbf{x}, t) &= U_0 t^2 \cos(\kappa x) \sin(\kappa y) \sin(\kappa z) \\ v(\mathbf{x}, t) &= U_0 t^2 \cos(\kappa x) \sin(\kappa y) \sin(\kappa z) \\ w(\mathbf{x}, t) &= 0 \\ P(\mathbf{x}, t) &= 0 \end{aligned} \quad (A-3)$$

satisfies the laminar Navier Stokes equations as programmed in the FAA code. See the results section for details of the above solution. Given the assumed manufactured solution in equation A-3 and the momentum equation A-1, the momentum source terms are,

$$\begin{aligned} S_{mom,1} &= U_0 t^2 \kappa^2 \mu \sin(\kappa x) \cos(\kappa y) \sin(\kappa z) \\ &+ 2U_0 t \rho \cos(\kappa x) \sin(\kappa y) \sin(\kappa z) \\ &+ 4U_0 t^2 \kappa^2 \mu \cos(\kappa x) \sin(\kappa y) \sin(\kappa z) \\ &+ 2U_0^2 t^4 \kappa \rho \cos^2(\kappa x) \cos(\kappa y) \sin(\kappa y) \sin^2(\kappa z) \\ &- 2U_0^2 t^4 \kappa \rho \cos(\kappa x) \sin(\kappa x) \sin^2(\kappa y) \sin^2(\kappa z) \end{aligned} \quad (A-4a)$$

$$\begin{aligned} S_{mom,2} &= U_0 t^2 \kappa^2 \mu \cos(\kappa x) \sin(\kappa y) \sin(\kappa z) \\ &+ 2U_0 t \rho \cos(\kappa x) \sin(\kappa y) \sin(\kappa z) \\ &+ 4U_0 t^2 \kappa^2 \mu \cos(\kappa x) \sin(\kappa y) \sin(\kappa z) \\ &+ 2U_0^2 t^4 \kappa \rho \cos^2(\kappa x) \cos(\kappa y) \sin(\kappa y) \sin^2(\kappa z) \\ &- 2U_0^2 t^4 \kappa \rho \cos(\kappa x) \sin(\kappa x) \sin^2(\kappa y) \sin^2(\kappa z) \end{aligned} \quad (A-4b)$$

$$S_{mom,3} = U_0 t^2 \kappa^2 \mu \cos(\kappa z) [\cos(\kappa x) \cos(\kappa y) - \sin(\kappa x) \sin(\kappa y)] \quad (A-4c)$$

where $S_{mom,i}$ are the source terms of the x_i - momentum equations. Similarly, the continuity equation source term associated with the solution of A-3 is,

$$S_{cont} = U_0 t^2 \kappa \sin(\kappa z) [\cos(\kappa x) \cos(\kappa y) - \sin(\kappa x) \sin(\kappa y)] \quad (A.5)$$

A.5 RESULTS.

This section documents the comparison of manufactured solutions and predicted results. All results are presented for a cubic domain Ω where $x \in [-0.5, 0.5]$, $y \in [0, 1]$ and $z \in [0, 1]$. Although nonorthogonal grids are possible with this code, they were not used for the verification results presented here. Section A.5.1 contains a direct comparison of the predicted and manufactured solutions.

A.5.1 Comparative Verification.

The results presented here are intended to demonstrate comparative verification of the code. Comparative verification means that the results look good. A comparison is made for the transient manufactured solution given by,

$$\begin{aligned}
 u(\mathbf{x}, t) &= U_0 t^2 \cos(\kappa x) \sin(\kappa y) \sin(\kappa z) \\
 v(\mathbf{x}, t) &= U_0 t^2 \cos(\kappa x) \sin(\kappa y) \sin(\kappa z) \\
 w(\mathbf{x}, t) &= 0 \\
 P(\mathbf{x}, t) &= 0
 \end{aligned}
 \tag{A-6}$$

where u , v , and w are the x , y , and z velocity and P is the thermodynamic pressure. In equation A-6, κ is the spatial wave number and describes how rapidly the solution varies spatially. For the problems of this section, $\kappa = \pi$ was chosen. Hence, one wavelength is completed in 2 spatial units. Smaller spatial wavenumbers could be used, however, a finer spatial discretization would be required to achieve asymptotic convergence (a result that will be used later). For the first case shown here, $U_0 = 0.1$ is used for this case to ensure diagonal positivity. Thus, up-winding is not “turned-on” and the operator is (spatially) second-order. As implemented in the FAA smoke transport code, up-winding results in a (spatially) first-order convergence.

Figures A-1 and A-2 show the velocity and pressure fields as predicted by the FAA smoke transport code. Temporal and spatial discretizations of (constant) time step = 0.001 and a 21 by 21 by 21 spatial mesh (CFL = 1.9e-3) were used. Results are shown in the x-y plane at $z = 0.5$ (halfway between the x-y plane faces of the cube). Figure A-1 illustrates the predicted pressure and w velocity component for this case at $t = 1.0$. Note that these results agree reasonably well with the specified manufactured solution with both fields being nearly zero (equation A-6). Figure A-2 shows the predicted u and v velocities (those specified as spatially and temporally varying in the manufactured solution). Note that, as expected, both fields are symmetric about the vertical/horizontal lines and centered at the center of the domain. Contour lines are included to emphasize the symmetry of these variables. The accuracy of the predicted u and v velocities, relative to the manufactured solution where the differences between the predicted and manufactured solutions ($v_{pred} - v_{mms}$ and $u_{pred} - u_{mms}$) are shown, is illustrated in figure A-3.

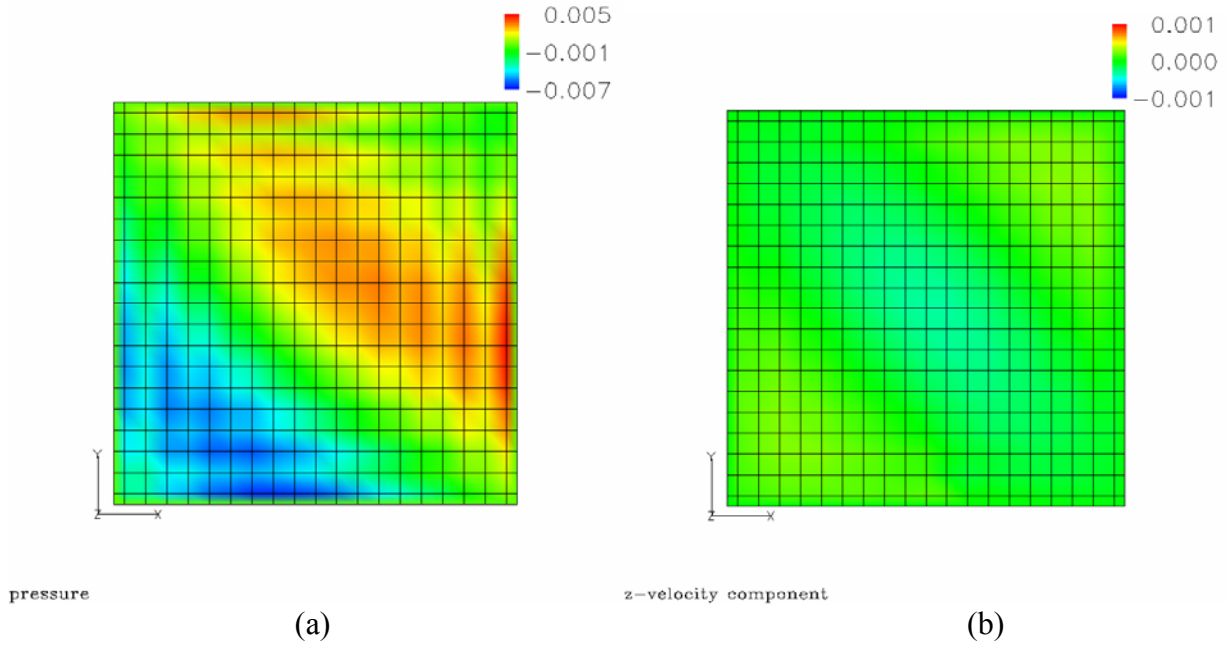


Figure A-1. Predicted (a) Pressure and (b) z-Velocity Component at Time = 1 for Manufactured Solution Case 1 With $U_0 = 0.1$

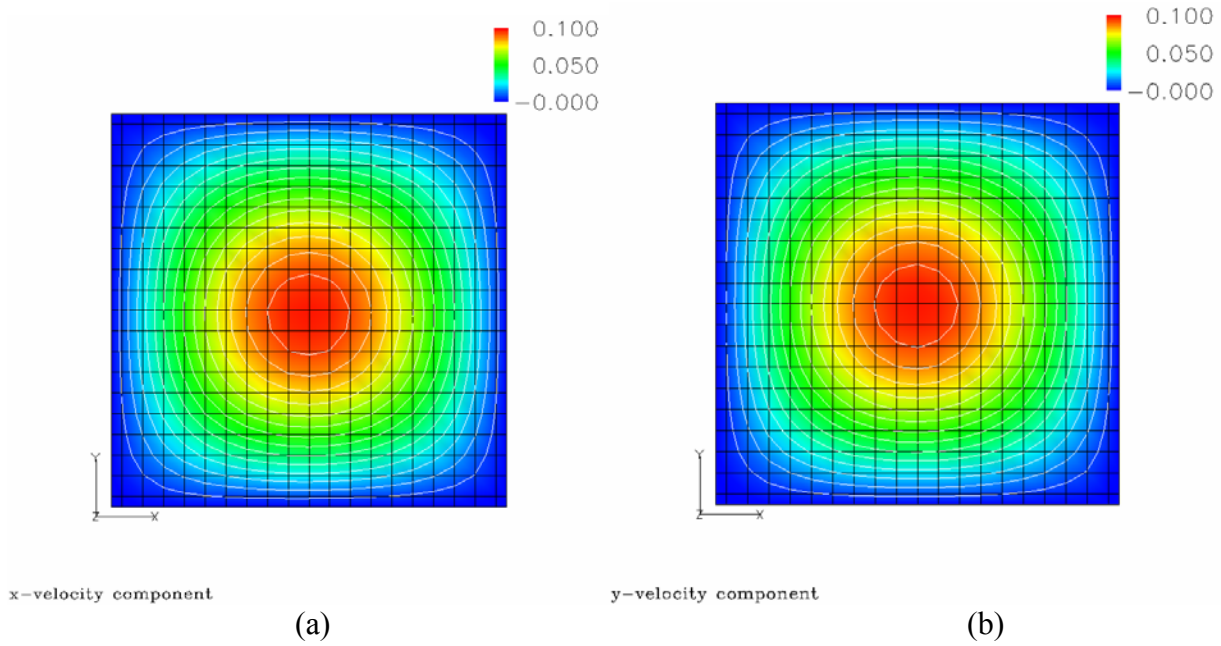


Figure A-2. Predicted (a) x-Velocity and (b) y-Velocity Components at Time = 1 for Manufactured Solution Case 1 With $U_0 = 0.1$

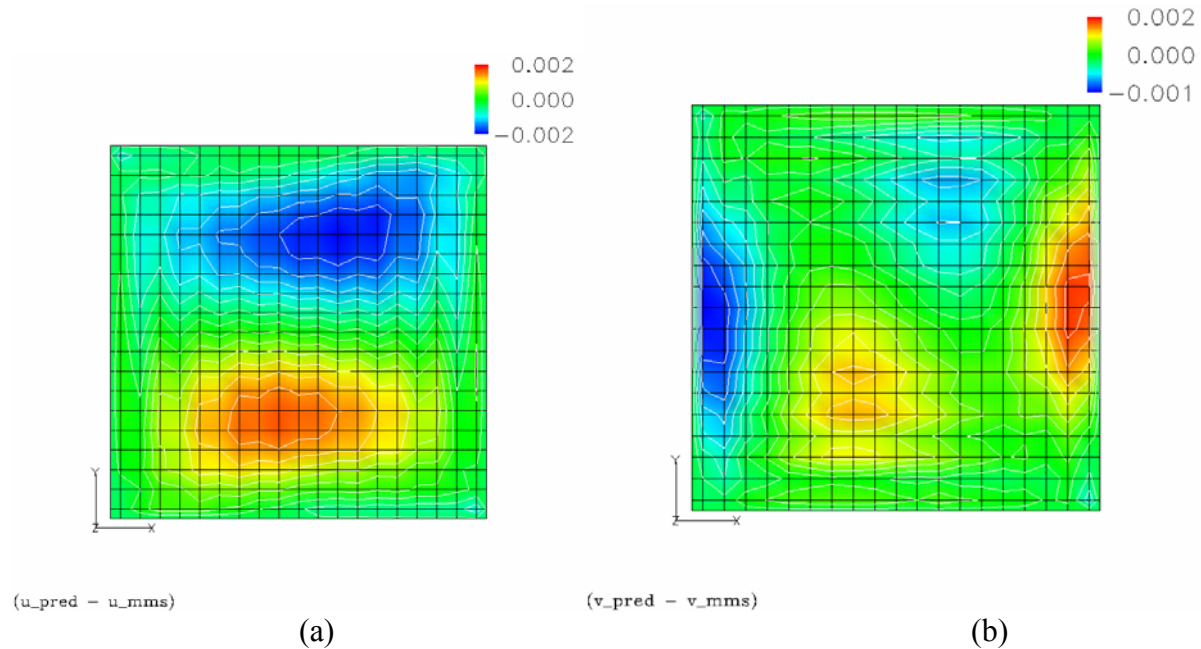


Figure A-3. Difference Between Predicted and Analytical (Manufactured Solution)
 (a) x-Velocity Component and (b) y-Velocity Component at Time = 1 for Manufactured Solution
 Case 1 With $U_0 = 0.1$

A.6 CONCLUSIONS AND RECOMMENDATIONS.

The results presented here indicate that the FAA smoke transport code is able to reasonably reproduce the analytical (manufactured) solution, as shown in table A-1. A more rigorous verification procedure is possible by examining convergence rates of the field variables in time and space at a variety of mesh refinements.

Table A-1. Maximum Errors in Field Variables for the Manufactured Solution With $U_0 = 0.1$

Mesh	Δ	$\max P_{pred} - P_{mms} $	$\max u_{pred} - u_{mms} $	$\max v_{pred} - v_{mms} $	$\max w_{pred} - w_{mms} $
21 by 21 by 21	5.263e-2	6.525e-3	2.254e-3	1.732e-3	8.377e-4